JOURNAL OF GEOPHYSICAL RESEARCH, VOL. 115, D00I10, doi:10.1029/2009JD012358, 2010

Transient climate simulations from the Maunder Minimum to present day: Role of the stratosphere

T. Spangehl,[1] U. Cubasch,[1] C. C. Raible,[2,3] S. Schimanke,[1] J. Körper,[1] and D. Hofer[2,3]

Received 29 April 2009; revised 2 October 2009; accepted 2 November 2009; published 10 March 2010.

[1] Transient climate simulations are performed covering the period from 1630 to 2000. A vertically extended version of a coupled atmosphere-ocean general circulation model is used, including a detailed representation of the stratosphere. One simulation is driven by changes in total solar irradiance due to solar activity as well as volcanic eruptions and changes in greenhouse gas (GHG) concentrations. A second simulation additionally includes changes in short-wave heating due to prescribed photochemical changes in ozone. The simulations are compared with reconstructions and other simulations employing less resolved stratosphere. The inclusion of the higher resolved stratosphere plays only a moderate role for the simulated climate variability on the hemispheric scale. Larger implications are found for regional scales. Both simulations reveal a shift of the North Atlantic Oscillation toward a more positive phase from the Maunder Minimum to present day, mainly attributed to anthropogenic increase in concentration of well-mixed GHG. Increase in GHG is related to a more disturbed stratospheric polar vortex resulting in an only moderate strengthening of tropospheric westerlies over Europe compared with the tropospheric version of the model. On multidecadal to centennial time scales the stratospheric solar forcing substantially contributes to the climate change signal in the stratosphere, and there is clear evidence for an impact on the tropospheric circulation.

Citation: Spangehl, T., U. Cubasch, C. C. Raible, S. Schimanke, J. Körper, and D. Hofer (2010), Transient climate simulations from the Maunder Minimum to present day: Role of the stratosphere, *J. Geophys. Res.*, *115*, D00I10, doi:10.1029/2009JD012358.

1. Introduction

[2] It is widely accepted that climate model simulations are in the range of reconstructions with respect to representation of the Northern Hemisphere (NH) mean near-surface temperature evolution of the last millennium [*Intergovernmental Panel on Climate Change* (*IPCC*), 2007]. However, much uncertainty remains with respect to the amplitude of the reconstructed and simulated climate anomalies, encouraging discussion about how realistic the simulations and reconstructions are [*von Storch et al.*, 2004; *Bürger et al.*, 2006; *Mann et al.*, 2007a, 2007b; *Zorita et al.*, 2007; *Christiansen et al.*, 2009].

[3] Reconstructions are based on statistical models utilizing regression techniques to relate information from proxy data to meteorological parameters. These methods are subject to a number of uncertainties. *Bürger et al.* [2006] emphasize that the level of uncertainty in a crucial manner depends on the representativeness of the calibration period. Moreover, as proxy data for near-surface temperature reveal sparse spatial density when going backward in time an important factor for the quality of the reconstructions is the spatial representativeness of individual proxies. By contrast, simulations are discussed with respect to uncertainties in model formulation and the individual experimental setup [e.g., *Osborn et al.*, 2006]. Uncertainties of the forcing data (usually proxy related) also have to be taken into account [*Rind et al.*, 2004; *Yoshimori et al.*, 2005, 2006]. A number of transient simulations using different atmosphere-ocean general circulation models (AO-GCMs) with prescribed natural and anthropogenic forcing cover the last 500 to 1000 years [e.g., *Zorita et al.*, 2004; *Ammann et al.*, 2006; *González-Rouco et al.*, 2006; *Stendel et al.*, 2006; *Casty et al.*, 2007; *Tett et al.*, 2007]. Of special interest is the Maunder Minimum (1645–1715, hereafter referred to as MM) where telescope-based observations show the nearly complete absence of sunspots, indicating a long phase of low solar activity. Some of the simulations were driven with a comparably large amplitude of the solar forcing (around 0.25–0.3% increase in total solar irradiance (TSI) from MM until present day) deduced from empirical estimates and Sun-like star comparison [e.g., *Hoyt and Schatten*, 1993; *Lean et al.*, 1995]. Newer estimates of TSI changes from the Maunder Minimum until present day based on physical models of the Sun are on the order of 0.1% [*Wang et al.*, 2005; *Krivova et al.*, 2007]. In addition, the role of the solar forcing compared to other relevant forcings (e.g., changes in greenhouse gas (GHG) concentrations) is still under discussion [cf. *Zorita et*

[1]Institut für Meteorologie, Freie Universität Berlin, Berlin, Germany.
[2]Climate and Environmental Physics, Physics Institute, University of Bern, Bern, Switzerland.
[3]Oeschger Centre for Climate Change Research, Bern, Switzerland.

0148-0227/10/2009JD012358$09.00

al., 2007, and references therein]. Here an important factor is the sensitivity of the climate model to the forcing [*Kelly and Wigley*, 1992], which may also depend on aspects of model formulation such as vertical resolution [e.g., *Rind et al.*, 1998].

[4] An important question is how far the simulated and reconstructed global and regional climate anomalies can be explained by external forcing or internal variability of the climate system. The picture becomes more complicated as regional climate anomalies may considerably differ from global mean temperature evolution. This aspect is emphasized by *Shindell et al.* [2001], who present a reconstruction of NH near-surface temperature that reveals strong cooling over NH midlatitudinal continental areas during MM when compared to a pre-industrial time period with higher solar activity. By contrast, the reconstruction reveals only moderate cooling during MM on the hemispheric scale as the strong continental cooling is partly compensated by warmer temperatures over northwestern oceanic basins. The authors show that a similar response in near-surface temperature is simulated when utilizing an atmosphere GCM that includes a detailed representation of the stratosphere and parameterized photochemical ozone chemistry, all coupled to a slab ocean. In their simulation, solar-induced changes in stratospheric heating rates result in a less equatorward deflection of upward propagating planetary waves, a strengthening of the Brewer-Dobson circulation and a shift of the Arctic Oscillation/North Atlantic Oscillation (AO/NAO) to a more negative phase contributing to the low European winter temperature during MM. Their mechanism is similar to what is known from 11 year cycle studies based on both reanalysis data and simulations [e.g., *Kuroda and Kodera*, 2002; *Matthes et al.*, 2006], highlighting the role of a detailed representation of the stratosphere for long-term climate simulations. Lower AO/NAO index values during MM are also found when driving the model with both changes in solar activity and volcanic eruptions, indicating that volcanic forcing during MM counteracts solar forcing on the shorter time scale, whereas solar forcing dominates on multidecadal time scales [*Shindell et al.*, 2003].

[5] The response in large-scale atmospheric circulation reveals more variety in the transient simulations. These simulations include deep ocean dynamics but only a simplified representation of the stratosphere. *Zorita et al.* [2004] find a response in AO/NAO during MM similar to *Shindell et al.* [2001, 2003] in a transient simulation covering the last 500 years performed with ECHO-G, but also emphasize the highly variable nature of the NAO. *Stendel et al.* [2006] find changes in atmospheric blocking situations during MM (especially in spring) in a transient simulation with ECHAM4-OPYC3 (1500–2000 AD) with some similarity to the reconstruction by *Luterbacher et al.* [2001]. *Yoshimori et al.* [2005] find a positive NAO response to volcanic forcing during MM only the first and second winter after eruption in an ensemble of simulations for MM. Using the same simulations as *Yoshimori et al.* [2005], *Raible et al.* [2007] find a more negative NAO response during MM when compared to a 1990 control climate which is attributed to solar and GHG forcing. A different study based on reconstructions and transient model simulations focusing on the time period from 1766 AD onward does not find a clear (linear) response to solar/volcanic forcing and emphasizes the high internal variability of the NAO [*Casty et al.*, 2007]. Using a coupled AO-GCM, *Bengtsson et al.* [2006] reveal evidence that the amplitude of climate fluctuations in Europe during the pre-industrial era (1500–1900 AD) can be explained by internal variability from a control simulation under constant pre-industrial conditions. However, it should be noted that also the timing of the climate anomalies is of relevance. This timing may be affected by varying external forcing factors such as solar variability and volcanic activity.

[6] Moreover, the anthropogenic increase in GHG concentrations during industrialization may play a role for the NAO. Using time-slice experiments with an atmosphere GCM including the middle atmosphere driven by prescribed sea surface temperature (SST), total and spectral solar irradiance (TSI/SSI), ozone and GHG, *Langematz et al.* [2005] find a shift of the NAO index from MM to present day toward its positive phase. Besides the direct solar impact on stratospheric temperatures, they also highlight the role of changes in GHG concentrations and dynamic troposphere-stratosphere interaction for the change in tropospheric circulation. A number of coupled AO-GCMs respond with a slight shift of the NAO toward a more positive phase to increasing GHG concentrations as shown by, for instance, *Osborn* [2004] and *Stephenson et al.* [2006], based on idealized experiments (with a 1% CO_2 increase until doubling of CO_2 concentration). *Baldwin and Dunkerton* [2001] emphasize the role of the dynamic troposphere-stratosphere coupling for climate. On the basis of reanalysis data, they find a downward propagation of wind anomalies from the stratosphere to the troposphere for phases of strong/weak polar vortex. *Sigmond et al.* [2004] reveal evidence for dynamic changes in the stratosphere under increased CO_2 concentrations in slab ocean experiments. Moreover, there is an increased number of sudden stratospheric warmings (SSWs) in an ensemble of SRES-A2 scenario simulations at the end of the 21st century compared with the end of the 20th century [*Huebener et al.*, 2007]. In this ensemble experiment the more disturbed NH stratospheric polar vortex leads to only a moderate increase and a more southward position of the tropospheric westerlies when simulations are compared with those where dynamic troposphere-stratosphere coupling effects are not well represented.

[7] In this study we perform transient simulations covering the time period from 1630 to 2000 using a coupled AO-GCM including the middle atmosphere. Simulations are compared with both reconstructions and model simulations with less-resolved stratosphere. The aim is to explore the role of the middle atmosphere for both the NH mean near-surface temperature time series and the simulated regional evolution of climate with special emphasize on the North Atlantic European sector. The focus is on (1) the direct stratospheric solar forcing via solar induced changes in stratospheric ozone and corresponding changes in heating rates and (2) dynamical coupling processes between the troposphere and stratosphere/mesosphere.

[8] The paper is structured as follows: The models, data and methods are explained in section 2. In section 3 the simulated NH near-surface climate, in particular the temperature evolution, is assessed in the different simulations and compared with reanalysis and proxy-based reconstructions addressing the extent to which differences in model

formulation and forcing functions play a role. Moreover patterns of simulated climate change during MM compared with (1) a pre-industrial time period with higher solar activity and (2) present-day climate are discussed with special emphasis on the NAO. Section 4 focuses on the vertical structure of simulated climate change, in particular on the role of the strength of the stratospheric polar vortex for changes in tropospheric circulation. Finally, our results are discussed and compared with other studies in section 5.

2. Models and Data

2.1. EGMAM and ECHO-G

[9] The main research tool of this study is the coupled AO-GCM EGMAM (ECHO-G with Middle Atmosphere Model) based on the AO-GCM ECHO-G (ECHAM4/HOPE-G) [cf. *Legutke and Voss*, 1999]. The atmospheric component is ECHAM4 [*Roeckner et al.*, 1996] extended for the middle atmosphere (also known as MA-ECHAM4). The spatial resolution of the atmosphere is T30/L39 (approximately 3.75° × 3.75° and 39 levels) with the top level located at 80 km (0.01 hPa) compared to T30/L19 and 30 km (10 hPa) in ECHO-G. The vertically extended atmosphere model includes changes in the parameterization of gravity waves, changed horizontal diffusion and minor modification in the radiation code [*Manzini and Farlane*, 1998]. Furthermore the setting of cloud parameters is marginally changed compared to ECHO-G. The oceanic component is HOPE-G (Hamburg Ocean Primitive Equation Global Model) with a spatial resolution of T42/L20 covering the deep ocean with a refined horizontal resolution near the equator of up to 0.5° in latitude. It includes a dynamic sea ice module representing drift ice [*Wolff et al.*, 1997]. The ocean component and coupling of the ocean and atmosphere are not changed compared to ECHO-G. To prevent climate drift EGMAM and ECHO-G use flux correction terms for heat and freshwater that are constant in time and reveal vanishing global mean values. Representation of land surface and soil processes is similar to that used by *Roeckner et al.* [1996]. ECHO-G was used for a number of climate variability and climate change studies [e.g., *Raible et al.*, 2001; *Zorita et al.*, 2004, 2005; *Cubasch et al.*, 2005; *Min et al.*, 2005a, 2005b; *González-Rouco et al.*, 2006; *Huebener et al.*, 2007; *Kaspar et al.*, 2007] and contributed to the Fourth IPCC Assessment Report [*IPCC*, 2007] (referred to as IPCC-AR4 hereafter). Using ensemble simulations forced with anthropogenic changes in GHG concentrations, *Huebener et al.* [2007] show that EGMAM simulates a near-surface climate that is close to ECHO-G when compared to reanalysis data. However, they report that inclusion of the middle atmosphere substantially improves the simulation of the climate in the upper troposphere/lower stratosphere in comparison with ECHO-G. Note that the model does not simulate a quasi-biennial oscillation (QBO) resulting in predominantly easterly winds in the tropical lower stratosphere. EGMAM simulates a decrease in circulation of the deep ocean as a response to increase in GHG concentration. As shown by *Körper et al.* [2009] for the A1B and B1 scenario, the projected decrease of the North Atlantic meridional overturning circulation (MOC) in EGMAM is similar in magnitude to the projected decrease of the multi model mean shown in IPCC-AR4.

[10] In the present study the EGMAM model is used to perform transient simulations covering the time period from 1630 to 2000. The simulations are driven by time-dependent changes in TSI representing solar variability and volcanic activity according to *Crowley* [2000]. The estimated change in TSI due to changes in solar activity is scaled to match the variance from *Lean et al.* [1995] during the 20th century, thus representing a rather strong 0.3% increase from the Maunder Minimum to present day. Changes in GHG concentrations are estimated from analysis of air bubbles trapped in Antarctic ice cores [*Etheridge et al.*, 1996; *Blunier et al.*, 1995]. The forcing series used (see Figure 1a) were already applied in a number of transient simulations with the ECHO-G model [e.g., *González-Rouco et al.*, 2006]. For the first simulation (hereafter referred to as EGMAM-1) we use fixed prescribed climatological ozone representing annual cycle variations only [*Brühl*, 1993]. A second simulation (EGMAM-2) additionally includes changes in stratospheric ozone concentration due to changes in solar activity. Here the effect of reduced photochemical ozone production during the Maunder Minimum compared with late 20th century solar activity is estimated on the basis of offline calculations as described by *Langematz et al.* [2005]. The resulting ozone anomaly reveals an increase in annual mean stratospheric ozone concentration of up to 6 percent from Maunder Minimum to present day (see Figure 1). Time-dependent changes in stratospheric ozone concentration and corresponding changes in stratospheric heating rates due to changes in solar activity are introduced by globally scaling the monthly ozone anomaly fields with respective changes in TSI from MM to late 20th century. As we use the standard radiation code in this simulation (only two intervals for the solar spectrum) [cf. *Roeckner et al.*, 1996], the additional effect on stratospheric heating rates due to changes in the UV part of the solar spectrum is not taken into account. The ozone climatology used as a background in EGMAM-2 is based on CIRA climatology and SBUV satellite measurements. Compared to the original CIRA/SBUV present-day (1980) ozone climatology, the background climatology is characterized by higher ozone concentration in the upper stratosphere, which accounts for the absence of anthropogenic aerosols. Note that the ozone field also excludes the ozone hole in the lower Antarctic stratosphere occurring since the late 1970s [cf. *Langematz et al.*, 2005]. Therefore, the ozone climatology used here as a background represents pre-industrial conditions. Both simulations are started from the same initial conditions taken from a long pre-industrial control simulation. To adapt to 1630 conditions, the simulations are integrated for another 100 years before the transient runs are started (the new background ozone climatology was used 50 years before the transient simulation started).

[11] For a systematic analysis of the role of the stratosphere, results are compared with a number of other simulations that were performed with the ECHO-G and Community Climate System Model version 3 (CCSM3) climate models. Two ECHO-G simulations are driven with the same forcings as EGMAM for 1630 to 1990 (time-dependent TSI and GHG), but in contrast to our simulations they cover the complete last millennium and are started from different initial conditions [cf. *González-Rouco et al.*, 2006]. The first simulation (hereafter referred to as ERIK1) was

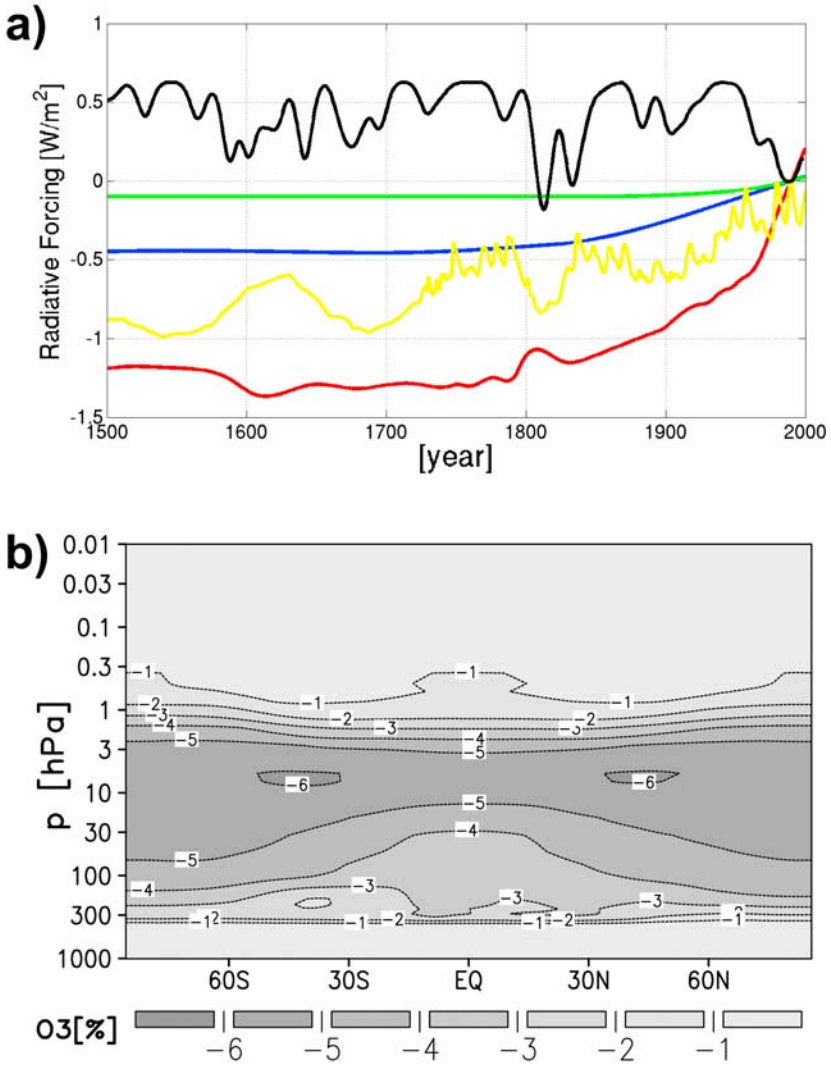

Figure 1. Forcings used to drive the simulations. (a) Solar (yellow), volcanic (black), CO_2 (red), CH_4 (blue), and N_2O (green) used for EGMAM and ECHO-G. The forcing is represented after conversion to the equivalent radiative forcing assuming the planetary albedo of 0.3 and using the simplified formula given by *Ramaswamy et al.* [2001, Table 6.2.]. Forcings are referenced to 1990 AD and volcanic forcing is smoothed with a Gaussian-weighted filter to remove fluctuations on time scales less than 30 years. (b) Solar-induced decrease of ozone (volume mixing ratio, percentage change) for Maunder Minimum when compared with present day as applied in EGMAM-2. Forcings for CCSM3 slightly differ from those used for EGMAM and ECHO-G and are shown by *Yoshimori et al.* [2010].

often criticized for atypical amplitudes in the simulated NH mean near-surface temperature, which is partly related to initialization from a comparably warm state [cf. *Osborn et al.*, 2006]. The second simulation (ERIK2) was started from a colder state and reveals lower cooling trends in the NH near-surface temperature from 1000 AD to 1700 AD [*González-Rouco et al.*, 2006]. Both simulations show a comparably strong temperature increase during the industrial era owing to the absence of anthropogenic sulphate aerosol forcing [*IPCC*, 2007].

2.2. CCSM3

[12] The second model is the National Center for Atmospheric Research CCSM3, which is a coupled model with no flux corrections [*Collins et al.*, 2006]. As ECHO-G, it consists of an atmosphere (Community Atmosphere Model version 3) [*William et al.*, 2006], an ocean (Parallel Ocean Program version 1.4) [*Smith and Gent*, 2004], a sea ice module (Community Sea Ice Model) [*Briegleb et al.*, 2004], and a land surface component (Community Land Model version 3) [*Oleson et al.*, 2004]. The model is used in its lowest resolution setting (T31gx3v5), which corresponds to a horizontal grid of 3.75° by 3.75° for the atmosphere and the land surface components, and a nominal resolution of 3° (3.6° in longitude and 0.6° to 2.8° in latitude) for the ocean and the sea ice components. In this configuration the atmosphere has 26 vertical levels up to 2 hPa. The ocean component has 25 layers with increasing thickness from the

surface to the bottom at 5000 m. Further information about the model and its components is provided at the CCSM web page (http://www.ccsm.ucar.edu/), and for the 1990 control climate simulation by *Yeager et al.* [2006].

[13] The CCSM3 is used to perform one perpetual 1500 AD control simulation and an ensemble of four transient experiments to simulate the climate from 1500 AD to 2000 AD. For both settings, the externally prescribed forcing consists of TSI, volcanic aerosols and GHG concentrations. As in the EGMAM model, solar variability is introduced via changes in TSI following *Crowley* [2000], but the scaling is slightly different, leading to an increase in TSI of 0.26% from the Maunder Minimum to today [*Yoshimori et al.*, 2010]. The volcanic aerosol concentration had also to be converted from the TSI changes from *Crowley* [2000] to total aerosol masses for the CCSM3, using the 6 strongest volcanic eruptions of the last 130 years [*Ammann et al.*, 2003]. The Crowley forcing shows tropical volcanic eruptions. To ensure that the aerosol concentration is higher in the tropics than in the mid and high latitudes, we latitudinally redistribute the volcanic aerosols by applying the cosine function to the aerosol concentration [*Yoshimori et al.*, 2010]. This aerosol is prescribed in the lower stratosphere uniformly during the year of the eruption. The GHG concentrations up to 1970 AD are based on work by *Etheridge et al.* [1996], *Blunier et al.* [1995], and *Flückiger et al.* [1999, 2002]. In the last 30 years, direct atmospheric measurements are used [*Dlugokencky et al.*, 2003; *Keeling and Whorf*, 2005; *Thompson et al.*, 2004]. Note that all forcing functions slightly differ from the forcing used in ECHO-G and EGMAM. The four ensemble simulations are started from different initial states derived from the control simulation [*Yeager et al.*, 2006; *Yoshimori et al.*, 2010; D. Hofer et al., manuscript in preparation, 2010]. The control integration has a small linear trend (as it was not a perfect equilibrium). This linear trend, estimated by a least-squared fit, is removed in the transient simulations.

3. Simulated Evolution of NH Near-Surface Climate

3.1. Comparison With Reanalysis

[14] To compare the simulated long-term mean near-surface patterns with observation based ERA40 reanalysis data [*Uppala et al.*, 2005], we use the metric introduced by *Taylor* [2001]. It is based on a relationship between the linear correlation coefficient, the magnitude of the standard deviation ratio and the bias-corrected root mean square error (RMSE) for two fields. In the polar coordinate system introduced by *Taylor* [2001] the angular coordinate denotes the correlation with observations and the radial coordinate shows the magnitude of the standard deviation ratio between the simulated and observed fields. It follows that the bias-corrected long-term mean RMSE is proportional to the distance of any model's point to the observed point (1, 0). As Figure 2 shows, all models are very close to reanalysis data with respect to the bias-corrected long-term mean (1961–1990) NH near-surface temperature fields during winter. Moreover, the simulations with EGMAM are closer to ECHO-G. Differences between the 4 individual simulations with CCSM3 are much smaller than the differences to both EGMAM and ECHO-G, indicating that the simulations with CCSM3 span a different cluster. A similar behavior is found for the bias in annual global mean near-surface temperature (not shown). All simulations reveal a slight bias with strongest biases for CCSM3 and smallest biases for the two simulations with EGMAM. This indicates that simulated near-surface temperature differences due to the inclusion of stratospheric processes are much smaller than (1) the model error and (2) differences due to other aspects of model formulation (e.g., differences between ECHO-G and CCSM3).

[15] A similar clustering is evident for the simulated mean sea level pressure (MSLP) patterns for the eastern North Atlantic/European sector defined here (Figure 2). Note that the area chosen agrees with available MSLP reconstructions (which will be discussed in section 3.3). The model including the stratosphere is closest to the reanalysis data. All models reveal high correlation for simulated MSLP fields when compared with ERA40 (linear correlation coefficient around 0.8), showing that they capture the general structure of the MSLP fields very well. In standard deviation ratio the larger differences indicate stronger deviation in the amplitude of the simulated long-term mean MSLP patterns between the different simulations (cf. Figure 2). Note that results for MSLP are sensitive to the exact area chosen and therefore less robust than for near-surface temperature (not shown).

3.2. NH Mean Near-Surface Temperature Evolution

[16] The time series of the simulated annual NH mean near-surface temperature of the various simulations is shown in Figure 3. Comparison with the uncertainty range from IPCC-AR4 given for reconstructions of NH mean near surface temperature evolution of the last 500 years (grey shading in Figure 3) shows that our simulations are in the range of reconstructions before industrialization (~1860). EGMAM and ECHO-G reveal a comparatively strong temperature increase from the onset of industrialization until the end of the 20th century that may be related to the absence of anthropogenic sulphate aerosol forcing in these simulations as pointed out by *Osborn et al.* [2006] for ERIK1. However, CCSM3 reveals a weaker temperature increase, indicating that differences in model formulation and differences in the forcing functions may also play a role. Note that for the CCSM3 simulations anthropogenic sulphate aerosol forcing (direct and indirect effect) is also absent. The transient climate response (TCR), defined as the change in annual global mean temperature after doubling of CO_2 concentration, may be used as a measure for the climate sensitivity of a model [*Cubasch et al.*, 2001]. The values are 1.5 K for EGMAM [*Körper et al.*, 2009], 1.7 K for ECHO-G (IPCC-AR4) and 1.4 K for CCSM3 [*Kiehl et al.*, 2006]. All models reveal a similar TCR when compared with the multi model ensemble shown in IPCC-AR4. The lower amplitude of the simulated NH near-surface temperature evolution for CCSM3 is partly explained by the low TCR of CCSM3. However, also differences in the forcing functions, such as the slightly lower amplitude in solar forcing used for CCSM3 may play a role. Moreover, differences in long-term climate response to different forcings and differences in initialization of the transient simulations have to be taken into account. While simulations with ECHO-G and CCSM3 cover the last 1000 and 500 years, respectively, radiation imbalances prior to 1630 AD are not included into the EGMAM simulations,

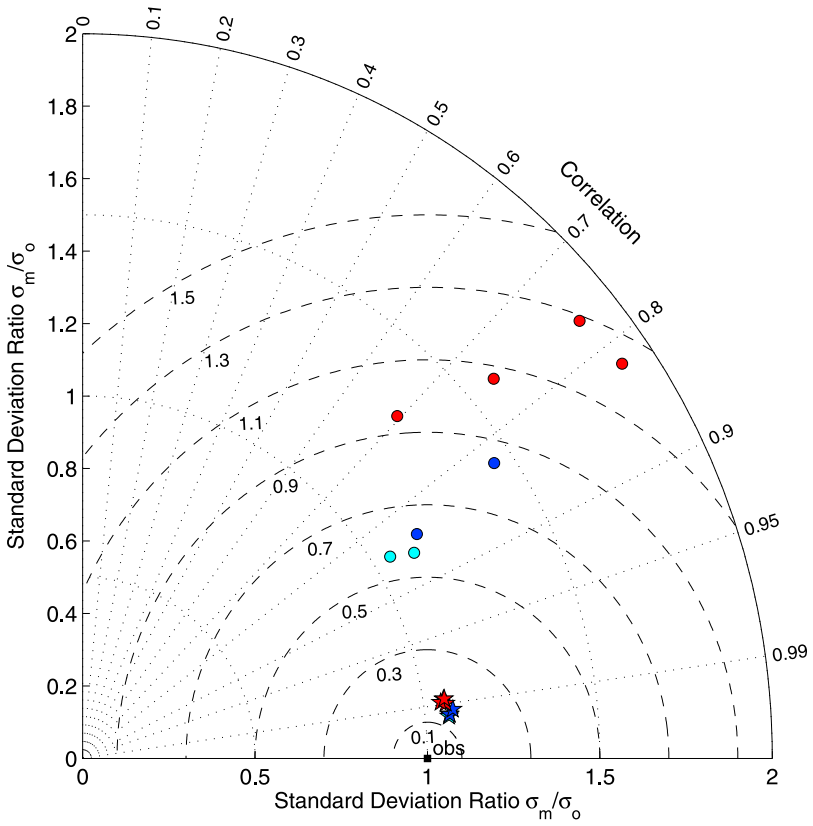

Figure 2. Taylor diagram: second-order statistics of simulated Northern Hemisphere near-surface temperature (star) and eastern North Atlantic/European MSLP (circle) for winter (DJF). The radial coordinate gives the magnitude of the standard deviation normalized by the observed value (ERA40). The angular coordinate gives the correlation with observations. Hence the distance between the observed value (obs) and any model's point is proportional to the centered RMS model error [cf. *Taylor*, 2001]. The geographical area for MSLP is 30°W–40°E, 30°N–70°N. All calculations refer to long-term winter mean fields (1961–1990 AD). EGMAM, cyan; ECHO-G, dark blue; CCSM3, red. Note that EGMAM stars disappear when stars for ECHO-G are plotted on top.

though they may play a role in the following century. Both simulations with EGMAM reveal a distinct cooling during MM; one simulation with ECHO-G (ERIK1) reveals a similar behavior, whereas all four simulations with CCSM3 show only moderate cooling during MM. This is in contrast to the Dalton Minimum (1790–1830, hereafter referred to as DM) where all simulations show a sharp cooling. Like MM, DM is also characterized by low solar activity; however, it reveals a comparatively strong volcanic forcing (see Figure 1a). *Wagner and Zorita* [2005] show for ensemble simulations with ECHO-G that the volcanic forcing is necessary to simulate a significant cooling during DM. The volcanic forcing, in particular the eruption of 1809 (unknown) and 1815 (Tambora), dominates also the temperature response during DM in the CCSM3 simulations. Other studies based on coupled AO-GCM simulations using comparably strong solar forcing reveal evidence for higher coherence between multidecadal scale solar variability and global/hemispheric scale near-surface temperature evolution [e.g., *Cubasch et al.*, 1997]. *Crowley* [2000] emphasizes that the Sun-climate correlations for the period 1000–1850 depend on the amplitude of the solar forcing and therefore vary substantially by the choice of the solar forcing.

[17] We conclude that differences between EGMAM and ECHO-G are significantly smaller than differences compared to CCSM3. This finding indicates that inclusion of stratospheric processes plays only a moderate role for the simulated NH-scale temperature evolution when compared with other uncertainties due to model formulation, forcing and experimental setup.

3.3. Regional Characteristics of the Winter Season (December-January-February)

3.3.1. Pre-industrial Near-Surface Temperature Change: Late Maunder Minimum Versus Pre-industrial (1716–1790)

[18] To investigate the role of natural forcing on climate we compare the Late Maunder Minimum (1675–1715, hereafter referred to as LMM) with a pre-industrial time period characterized by higher solar activity (1716–1790, named PI in the following). As suggested above, the simulations with EGMAM/ECHO-G are closer to each other than to simulations with CCSM3 with respect to representation of NH near surface temperature pattern. Therefore simulations are grouped into (1) 4 simulations with EGMAM/ECHO-G and (2) 4 simulations with CCSM3, enabling calculation of

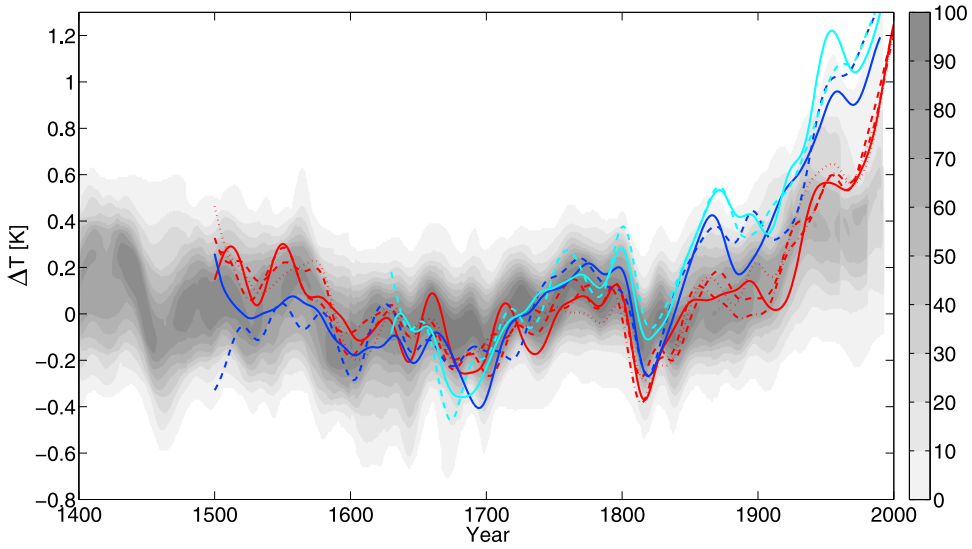

Figure 3. Annual Northern Hemisphere mean 2 m temperature anomaly (K) for simulations with EGMAM (EGMAM-1 fixed ozone, cyan/solid line; EGMAM-2 time-dependent ozone, cyan/dashed line), ECHO-G (ERIK1, dark blue/solid line; ERIK2, dark blue/dashed line), and CCSM3 (four individual realizations, red curves). Grey shading represents overlap of NH temperature reconstructions from IPCC-AR4. Data from reconstructions and simulations with ECHO-G, and CCSM3 are expressed as anomalies from their 1500–1899 means. Simulations with EGMAM are centered to 1716–1790 mean value from the centered (1500–1899) ECHO-G simulations. All time series are smoothed with a 30 year low-pass filter.

ensemble mean values (hereafter referred to as EEM for group 1 and CEM for group 2). Note that the related changes in the ensemble mean values reveal a better signal-to-noise ratio than the changes in individual simulations. In line with the annual temperature evolution (section 3.2) the winter (December–January–February (DJF)) temperature decrease during LMM is larger in EEM in most areas when compared to CEM (Figures 4a and 4b). Both groups reveal a statistically significant cooling over large parts of tropical ocean areas. However, less significant cooling is found over the equatorial Pacific, a region of high internal variability related to ENSO. Note that the clear lack of cooling around the eastern Pacific equatorial region found in EEM (Figure 4a) is also consistent with results from *Meehl et al.* [2009] who reveal evidence for a La Niña (El Niño) like response to eleven year solar cycle maximum (minimum) conditions. In EEM the strongest cooling is found over northern Europe/Asia, polar regions (in particular the Greenland-Iceland-Norwegian Seas), Sea of Okhotsk and also the western North Atlantic. By contrast, CEM reveals the strongest cooling to be north of Iceland. The North Atlantic/European region is characterized by cooling over Western Europe and warming over the central North Atlantic, which coincides with a change in ocean circulation. Hofer et al. (manuscript in

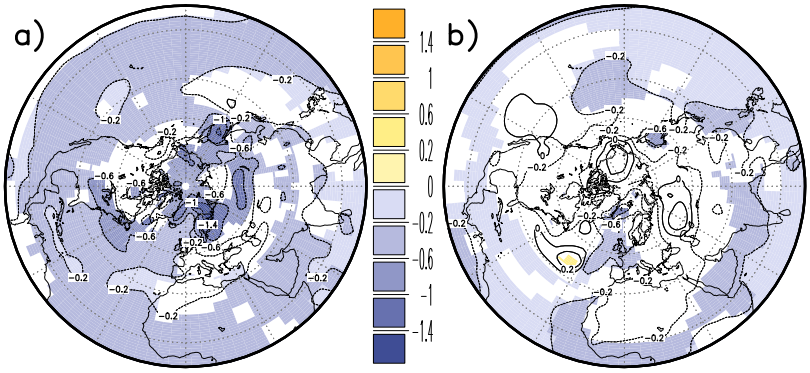

Figure 4. Long-term winter (DJF) ensemble mean difference of near-surface temperature (K) for LMM (1675–1715) minus PI (1715–1790) for (a) simulations EGMAM-1, EGMAM-2, ERIK1, and ERIK2 and (b) four simulations with CCSM3. Colored areas are statistically significant above 99th percentile value based on Student's *t* test (standard deviation calculated by averaging over variances and degree of freedom is taken as the sum over the individual realizations).

Table 1. Comparison of Northern Hemisphere 2 m Temperature Change Patterns: LMM Minus PI[a]

	EGMAM-1	EGMAM-2	ERIK1	ERIK2
EGMAM-1	1	0.4 (0.47)	0.26 (0.43)	0.23 (0.56)
EGMAM-2	0.4 (0.47)	1	0.3 (0.14)	0.29 (0.4)
ERIK1	0.26 (0.43)	0.3 (0.14)	1	−0.05 (0.07)
ERIK2	0.23 (0.56)	0.29 (0.4)	−0.05 (0.07)	1

[a]Linear pattern correlation coefficient for Northern Hemisphere 2 m temperature change patterns LMM minus PI of individual simulations contributing to ensemble mean shown in Figure 4a. Area weighting is applied. In brackets: all grid points normalized by standard deviation.

preparation, 2010) show that the mean MOC of the CCSM3 simulations is stronger during LMM than in the subsequent period 1715–1790.

[19] Comparison of the individual simulations from group (1) reveals that simulations with EGMAM are closer together than the two simulations with ECHO-G (see Table 1). Simulations with EGMAM are characterized by strong cooling in the western North Atlantic (similar to results from *Fischer-Bruns et al.* [2002] and *Zorita et al.* [2004] for a further simulation with ECHO-G) and north of Iceland and partly over Northern Europe (not shown). The strong cooling over the western North Atlantic is related to an increase in sea ice and a salinity anomaly; however, a significant change in ocean circulation (meridional overturning circulation) is not found (not shown). A clear NAO-like temperature response during LMM is only found in ERIK1 with strong cooling over northern parts of Eurasia and warming west of Greenland (not shown).

3.3.2. Changes of the NAO

[20] Principal component analysis (PCA) is applied to simulated winter mean MSLP for the North Atlantic/European sector to assess the ability of the different models to simulate NAO variability. PCA is calculated for each model separately, including all available data from the transient simulations (see Figure 5). Note that results were not sensitive to the exact time period chosen. For all models used in this study the leading mode (EOF1) reveals the well-known pressure seesaw, with the two centers being located around Iceland and the Iberian Peninsula (Cape Finisterre). Explained variance of EOF1 is higher in CCSM3 than in EGMAM and ECHO-G (Figure 5). EGMAM reveals somewhat less variance than ECHO-G around the southern center. Explained variance of EOF1 is slightly higher in EGMAM than in ECHO-G (similar results are found when restricting simulations with ECHO-G to the last 500 years). EGMAM shows more realistic variability of the NH stratospheric polar vortex when compared with the tropospheric version of the model [*Huebener et al.*, 2007]. Therefore this finding is in line with the concept that downward propagating wind anomalies from the stratosphere to the troposphere act as an additional source of tropospheric variability. In a current study [*Langematz et al.*, 2009] show that EGMAM reveals downward propagation of AO anomalies from the stratosphere to the troposphere resembling results for observations [e.g., *Baldwin and Dunkerton*, 2001].

[21] To investigate the time behavior of the NAO, a winter (DJF) index is constructed based on normalized pressure difference (reference period 1900–1980 [cf. *Jones et al.*, 1997]) between areas around Lisbon, Portugal (25°W–0°; 35°N–50°N) and Iceland (25°W–0°; 55°N–70°N). Besides high decadal to multidecadal variability there is a tendency in most simulations (with the exception of CCSM3-2) toward more positive NAO index values during the second half of the 20th century in comparison with the pre-indus-

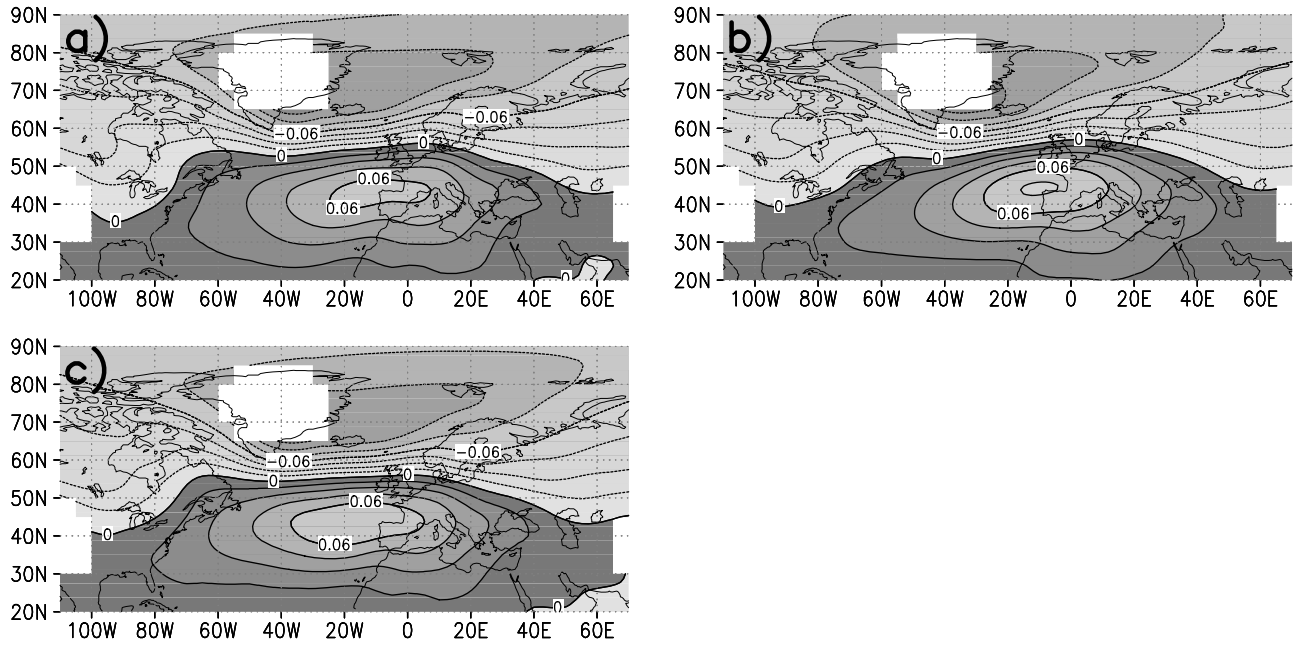

Figure 5. Leading mode (Eigenvector) of principal component analysis based on winter mean (DJF) MSLP for North Atlantic/European sector (grid points with orography more than 1500 m above sea level excluded) in the simulations for (a) EGMAM (two simulations, time period 1631 to 2000, 44.5% explained variance), (b) CCSM3 (four simulations, 1501 to 2000, 56.2%), and (c) ECHO-G (two simulations, 1001 to 1999 (ERIK1)/1990 (ERIK2), 41.2%). See text for further details on methods.

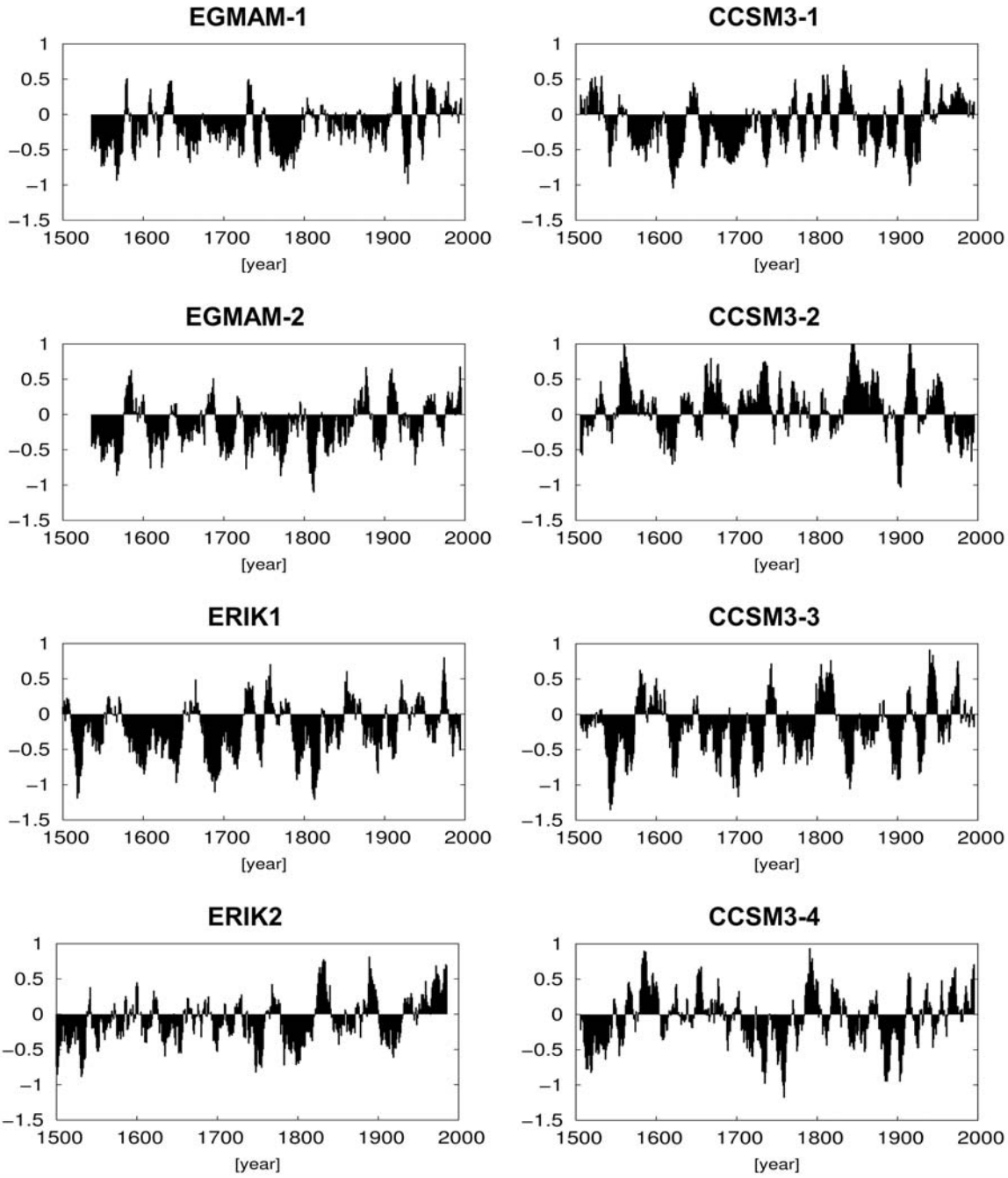

Figure 6. Winter (DJF) NAO indices for simulations with EGMAM (EGMAM-1, EGMAM-2), ECHO-G (ERIK1, ERIK2), and CCSM3 (CCSM3-1, CCSM3-2, CCSM3-3, CCSM3-4) calculated as normalized pressure anomalies (reference period 1900–1980 [cf. *Jones et al.*, 1997]) between 25°W–0°, 35°N–50°N and 25°W–0°, 55°N–70°N. All series are shown as centered 11 year running mean values. Years 1531–1630 for EGMAM-1 and EGMAM-2 are taken from corresponding control simulations.

trial era (Figure 6). With the exceptions of CCSM3-2 all simulations show a positive linear trend of the NAO from 1688 (absolute minimum in solar activity; see Figure 1a) toward the end of the simulation. However, trends are only statistically significant (above 90th percentile value after Mann-Kendall test) for EGMAM-1, EGMAM-2, ERIK2, CCSM3-3 and CCSM3-6. All simulations fail to capture the strength of the strong positive NAO trend during the second half of the 20th century [cf. *Raible et al.*, 2005] found in observational data (not shown). Note that *Zorita et al.* [2005] find a shift of the AO toward more positive values in ERIK1 by the end of the simulation. Idealized simulations of the tropospheric version of ECHAM4 show a strong NAO response to GHG forcing compared with a number of other models [*Stephenson et al.*, 2006]. As will be shown below, changes in MSLP from LMM to present day over the

North Atlantic/Europe are located eastward of the NAO centers of action in ERIK1, and therefore not very well represented in our NAO index. However, the near-surface temperature response in ERIK1 during LMM compared to the pre-industrial era (see section 3.3.1) is consistent with a shift of the NAO index toward more negative values during LMM. A similar shift is also evident during DM. ERIK2 reveals more negative NAO index values only during DM. Note that the NAO index is also more negative in LMM and late DM in EGMAM-2. More negative NAO index values during LMM are simulated in EGMAM-1, CCSM3-1, CCSM3-3. Note that the ensemble mean of all eight simulations also reveals more negative NAO index values during LMM (figure not shown). The ensemble mean of all four simulations with CCSM3 displays also more negative NAO index values for LMM. By contrast ensemble mean response for DM shows a tendency toward more positive NAO index values for CCSM3 (figure not shown). However, despite the more realistic volcanic forcing a clear NAO positive response to individual volcanic eruptions is not found in CCSM3. By contrast, EGMAM reveals a tendency toward more negative NAO values after strong volcanic eruptions (not shown) indicating that the tropospheric volcanic forcing (i.e., reduced incoming short-wave radiation and tropospheric cooling due to scattering of volcanic aerosols) may counteract the strengthening of the AO/NAO associated with tropical eruptions and heating of stratospheric layers [cf. *Rind et al.*, 2005]. However, as this is only a short-term effect and as there is only a very limited number of strong volcanic eruptions during LMM this effect might contribute but does not dominate the negative ensemble mean NAO response during LMM. These results indicate that the solar forcing dominates the NAO response during LMM. However, the absence of a shift toward more negative NAO index values during LMM in CCSM3-2, CCSM3-4 and ERIK2 and the absence of a clear response to volcanic forcing in CCSM3 also indicates that the high internal variability of the NAO is important for European winter climate variability during the pre-industrial era.

[22] To further investigate time behavior we apply a wavelet analysis that reveals the nonstationary character of the NAO spectrum (Figure 7). There is no coherence between the different simulations, and the characteristics of the wavelets of the forced simulations (Figure 7) are similar to those of the control simulations (not shown). However, there are some indications of a possible solar effect on the NAO variability. The simulation that also includes stratospheric solar forcing (EGMAM-2) reveals partly enhanced energy with a period of about 20 years during DM. However, it should be mentioned that enhanced energy with a period of about 20 years is also evident in the corresponding control simulation with EGMAM (e.g., Figure 7, EGMAM data for 1530–1629 taken from control simulation). Moreover, also the volcanic forcing reveals enhanced energy of 20 years during DM (not shown). EGMAM-2 reveals enhanced energy on multidecadal time scale also during LMM; however, in this respect the signal is not statistically significant when compared to noise (see Figure 7).

[23] One simulation with ECHO-G reveals statistically significant enhanced energy with a period of about 100 years during the pre-industrial era. Note that this signal extends back to 1500 when the complete NAO series from 1000 to 2000 is taken into account (figure not shown). A similar signal with enhanced energy with a period of approximately 100 years is also found in the solar TSI forcing series (see section 4, Figure 10), suggesting a response of the simulated NAO to solar forcing. A similar result with a somewhat phase-shifted NAO index series was already found by *Zorita et al.* [2004] for a 500 year transient simulation with ECHO-G (named COLUMBUS simulation in literature), using similar forcing series to those applied in this study. However, the time behavior of the second simulation with ECHO-G (ERIK2) differs: for example, no NAO response to solar forcing is found for MM. The wavelet spectra of NAO in the 4 simulations with CCSM3 reveal partly similar features as discussed for EGMAM and ECHO-G. It can be concluded that a solar effect on NAO is indicated especially in the simulations EGMAM-2 and ERIK1. However, a clear and consistent response in terms of a direct linear response of NAO to solar forcing is not found. This is in some agreement with results from *Casty et al.* [2007] for both reconstructed and simulated NAO indices for the time period from 1766 to 2000. Moreover, we conclude that better representation of the stratosphere is not necessary to obtain an NAO response to solar forcing during pre-industrial times if comparatively strong solar induced TSI changes are prescribed.

3.3.3. Long-Term Changes of MSLP: LMM Versus Present Day

[24] Though a clear and consistent solar effect on the NAO is not found, analysis of the simulated NAO indices indicates a systematic change from lower NAO values during LMM to higher NAO values at the end of the 20th century (see section 3.3.2). Here, the combined effect of changes in natural (solar, volcanic) and anthropogenic forcing (GHG) has to be taken into account. The simulated change pattern for MSLP from LMM to the present-day period 1960–1990 (hereafter referred to as PD) reveals a NAO-like pattern for the simulations with EGMAM and ECHO-G (Figures 8a–8d). The pattern correlation coefficient between the MSLP change patterns is 0.9 for simulations with ECHO-G (ERIK1, ERIK2) compared to 0.72 for EGMAM-1 and EGMAM-2 simulations (see Table 2), indicating that the change pattern is more robust in simulations with ECHO-G. However, change patterns of different realizations with the same model correlate higher than any pair of realizations with different models (see Table 2).

[25] EGMAM-2 is in best agreement with reconstruction after *Luterbacher et al.* [2002]; although the signal is too strong west of the British Isles. EGMAM-1 shows a weak change pattern in agreement with reconstruction (see ABS, Table 3), but does not capture the position of the centers (especially the northern center) very well (see RMSE, LINCORR, in Table 3). ERIK1 captures the shape of the pattern comparatively well (see LINCORR, Table 3) but overestimates its strength (see RMSE, ABS, Table 3). ERIK2 shows a generally weaker change pattern than ERIK1 (see ABS, Table 3, in better agreement with reconstruction); however, there are shortcomings with respect to the exact position and local strength of the change signal (see RMSE, LINCORR, Table 3). Additionally, there is evidence that ECHO-G overestimates the MSLP change in the Mediterranean when compared to EGMAM and reconstructions. For comparison with reconstruction it should

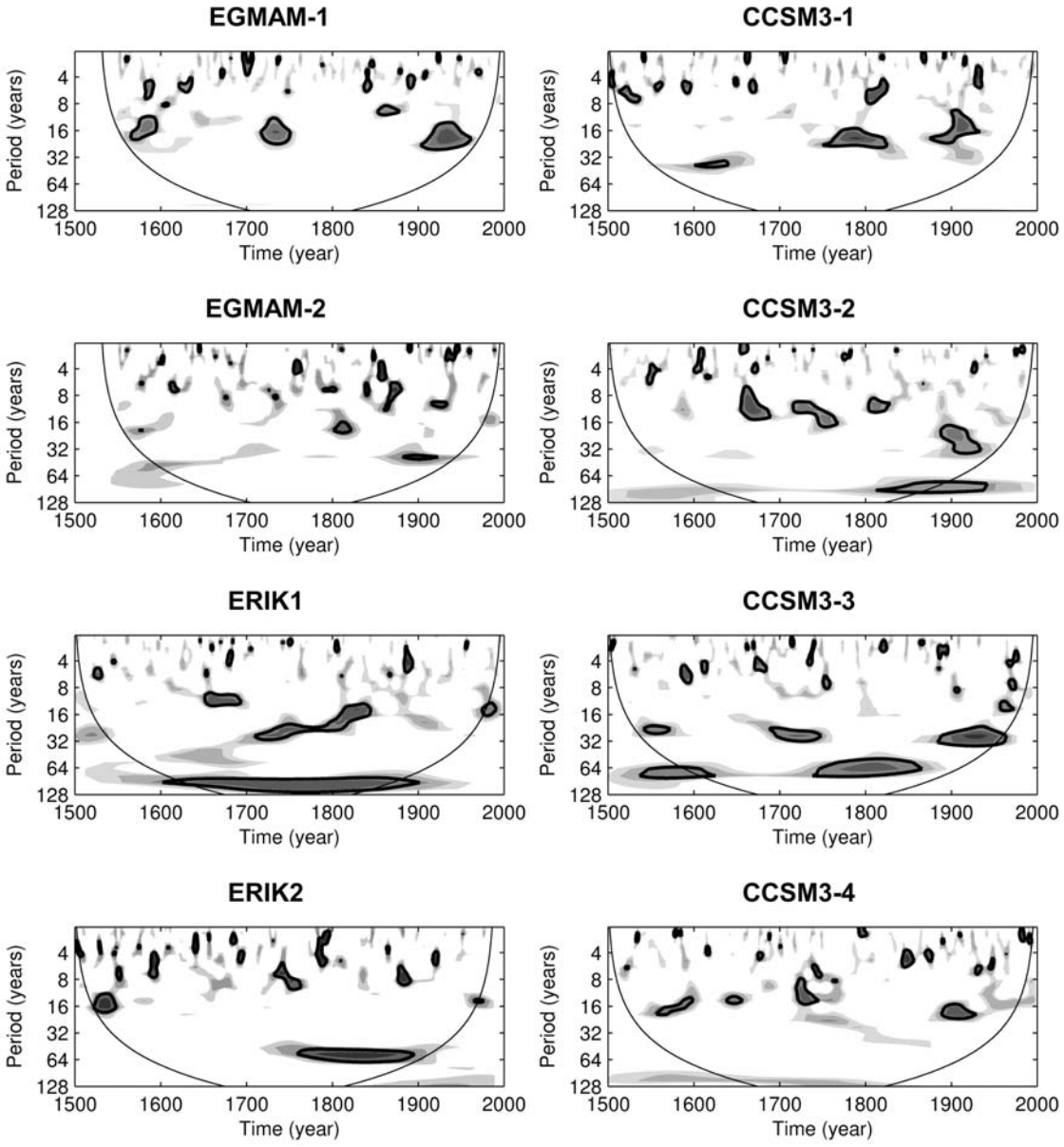

Figure 7. Wavelet power spectrum [after *Torrence and Compo*, 1998] of winter NAO indices for simulations with (left) EGMAM and ECHO-G and (right) CCSM3. The Morlet wavelet is used. The oval curve indicates area of confidence as the variance is underestimated outside of this border. Thick black lines show 95% level of statistical significance (based on chi square test following *Torrence and Compo* [1998] compared to stationary noise (redness estimate based on autocorrelation of the particular series).

be noted that both models do not include changes in anthropogenic sulphate aerosols and that the stratospheric solar forcing applied in EGMAM-2 does not explicitly include changes in the UV part of the solar spectrum. Furthermore, the quality of reconstructions may suffer under sparse spatial density of proxy data over ocean areas [e.g., *Casty et al.*, 2007]. The ensemble mean of CCSM3 also shows a NAO-like change pattern with a shift toward stronger zonal flow from LMM until PD in line with EGMAM/ECHO-G and reconstructions. In CCSM3 the pattern is shifted toward the Icelandic region, resulting in a somewhat weaker change over Europe when compared to EGMAM/ECHO-G and reconstructions (see Figure 8 and Table 3). Thus we conclude that the simulation including stratospheric processes and stratospheric solar ozone forcing best resembles the reconstructions with respect to simulated changes of the NAO from LMM to PD. The ensemble mean of EEM and CEM also performs comparatively well.

4. Vertical Structure and Stratospheric Variability

[26] As shown in section 3.3, a more realistic representation of the stratosphere improves the simulation of regional near surface climate to some extent. In the following we discuss the simulated climate change signal in the

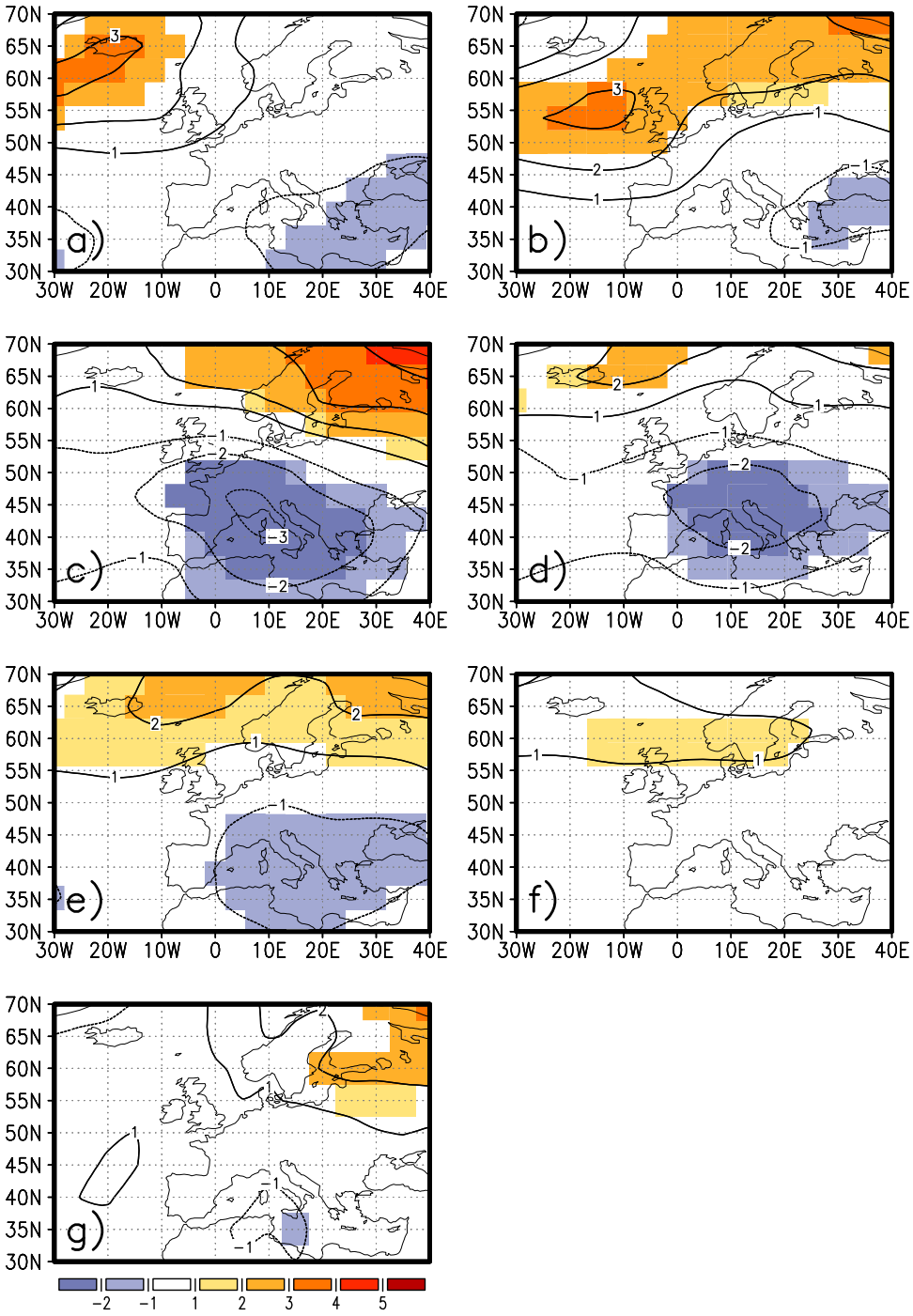

Figure 8. Long-term winter mean difference of MSLP (hPa) for LMM (1675–1715) minus PD (1960–1990) for (a) EGMAM-1, (b) EGMAM-2, (c) ERIK1, and (d) ERIK2; colored regions are statistically significant above 95th percentile value after Student's *t* test. (e) Ensemble mean of the four simulations with EGMAM/ECHO-G). (f) Ensemble mean of the four simulations with CCSM3. (g) Reconstruction after *Luterbacher et al.* [2002]. For *t* test of Ensemble, standard deviation calculated by averaging over individual variances and degree of freedom is taken as the sum over the individual realizations.

Table 2. Comparison of MSLP Change Patterns: LMM Minus PD[a]

	EGMAM-1	EGMAM-2	ERIK1	ERIK2
EGMAM-1	1	0.72	0.41	0.54
EGMAM-2	0.72	1	0.54	0.52
ERIK1	0.41	0.61	1	0.90
ERIK2	0.54	0.52	0.90	1

[a]Linear pattern correlation coefficient for MSLP change patterns shown in Figure 8. Area weighting is not applied.

stratosphere with special emphasis on the variability of the polar vortex.

[27] The simulation including solar stratospheric ozone forcing (EGMAM-2) simulates statistically significant lower annual mean zonal mean temperature in large parts of the troposphere during LMM when compared with PI (Figure 9a). The maximum cooling is found close to surface in NH mid-latitudes and in the upper tropical troposphere. Statistically significant cooling during LMM is also found in the tropical/subtropical stratosphere up to the stratopause. In the tropical stratosphere a minimum cooling is found between 100 hPa and 30 hPa, which is however not statistically significant. The boreal winter response shows a statistically significant decrease of the stratospheric temperature over lower latitudes and the complete summer hemisphere similar to results from 11 year solar cycle studies [e.g., *Kodera and Kuroda*, 2002]. However, a statistically significant difference of the strength of the Brewer-Dobson circulation and the polar stratospheric vortex is not found when comparing LMM with PI (therefore not shown).

[28] The difference of the zonal mean temperature between PD and LMM is dominated by tropospheric warming and radiative cooling in the stratosphere and lower mesosphere (Figure 9b). Similar change patterns are inferred from doubled-CO_2 experiments and scenario simulations with prescribed increase of GHG concentrations [e.g., *Rind et al.*, 1998; *Butchart et al.*, 2000] indicating that the change pattern from LMM to PD is dominated by increase of well mixed GHG concentrations. The maximum tropospheric warming is found over the Arctic close to surface and around the tropical tropopause region reaching a value of about 2 K (Figure 9b). The simulated temperature change for the higher troposphere and for the stratosphere is similar to that given by *Langematz et al.* [2005].

[29] Of special interest is the response during boreal winter. The difference between the climate change signals (PD minus LMM) from EGMAM-2 (the simulation including stratospheric solar ozone forcing) and from EGMAM-1 (the simulation that uses fixed climatological ozone) reflects the response to solar stratospheric ozone forcing. Solar induced ozone increase leads to higher temperatures in the stratosphere covering NH subtropics, tropics and the complete summer hemisphere (Figure 9c). On the basis of idealized climate model experiments, A. A. Scaife et al. (A stratospheric amplifier of regional climate change, submitted to *Nature Geoscience*, 2009) show that increase in CO_2 concentrations results in a southward shift of the polar night jet. The related changes in vertical wind shear and baroclinicity in the lower stratosphere/upper troposphere affect the strength and position of storm tracks leading to increased storm track activity over western Europe. Analysis of upper tropospheric baroclinicity in our simulations clearly shows that similar to the mechanism proposed by Scaife et al. (submitted manuscript, 2009) the combined GHG and solar effects result in increase of upper tropospheric baroclinicity west of the British Isles and related increase in storm tracks from LMM to PD thereby explaining the strong change in MSLP around the British Isles we find in EGMAM-2.

[30] The time behavior of the NH polar stratospheric vortex strength in EGMAM-1 reveals evidence for a more disturbed vortex at the end of the 20th century (Figure 10a). The difference in long-term mean strength of the polar vortex between the end of the 20th century (1981–2000) and the LMM (1675–1715) was tested by a Student's *t* test on a winter basis. We find a difference of 5 m/s, which is statistically significant above the 95th percentile value (Figure 10a). This indicates a weakening of the stratospheric polar vortex in EGMAM-1 by the end of the simulation. We also find a strengthening of the Brewer-Dobson circulation from LMM until the end of the 20th century. However, the related trend is not statistically significant (therefore not shown). The decrease in stratospheric polar vortex strength is related to an increase of GHG concentrations. A similar but even stronger change is found when using the same model for future climate projections under the IPCC SRES-A2 scenario as demonstrated by *Huebener et al.* [2007]. By analyzing ensemble simulations, they show that the more disturbed polar vortex is related to a rise in the number of sudden stratospheric warmings due to increasing stratospheric wave forcing from the troposphere. Moreover, they reveal evidence for an impact on the circulation in the troposphere. In another study, S. Schimanke et al. (manuscript in preparation, 2010) show that the GHG induced change is due to increased stratospheric wave forcing from the troposphere and poleward wave deflection in the middle atmosphere associated with a strengthening of the Brewer-Dobson circulation.

[31] The inclusion of solar stratospheric ozone forcing leads to higher multidecadal scale variability of the stratospheric polar vortex strength (Figures 10b and 10d). For DM enhanced energy is found for periods around 40–50 years where also the solar forcing reveals statistically significant enhanced energy (Figure 10d). Enhanced energy is also found for LMM, however with a shorter period than for the solar forcing (indicating a possible nonlinear effect). Note that a similar increase in multidecadal variability of the NH polar

Table 3. Simulated MSLP Change Patterns Versus Reconstruction: LMM Minus PD[a]

	RMSE	LINCORR	ABS
EGMAM-1	1.59 (1.35)	0.15 (0.28)	1.34 (0.99)
EGMAM-2	1.17 (0.9)	0.7 (0.68)	1.76 (1.26)
ERIK1	1.64 (1.32)	0.68 (0.68)	2.04 (1.52)
ERIK2	1.55 (1.38)	0.43 (0.44)	1.44 (1.09)
ENS-MEAN	1.11 (0.99)	0.61 (0.64)	1.33 (0.96)
CCSM3-MEAN	1.12 (1.1)	0.28 (0.36)	0.69 (0.50)
LUTERBACHER	0	1	1.17 (0.83)

[a]Root mean square error (hPa) (RMSE) and linear pattern correlation coefficient (LINCORR) of simulated MSLP change patterns shown in Figures 8a–8f versus reconstruction shown in Figure 8g. ABS: vector length (hPa) of the patterns shown in Figures 8a–8g. Area weighting is not applied (brackets show area weighted values).

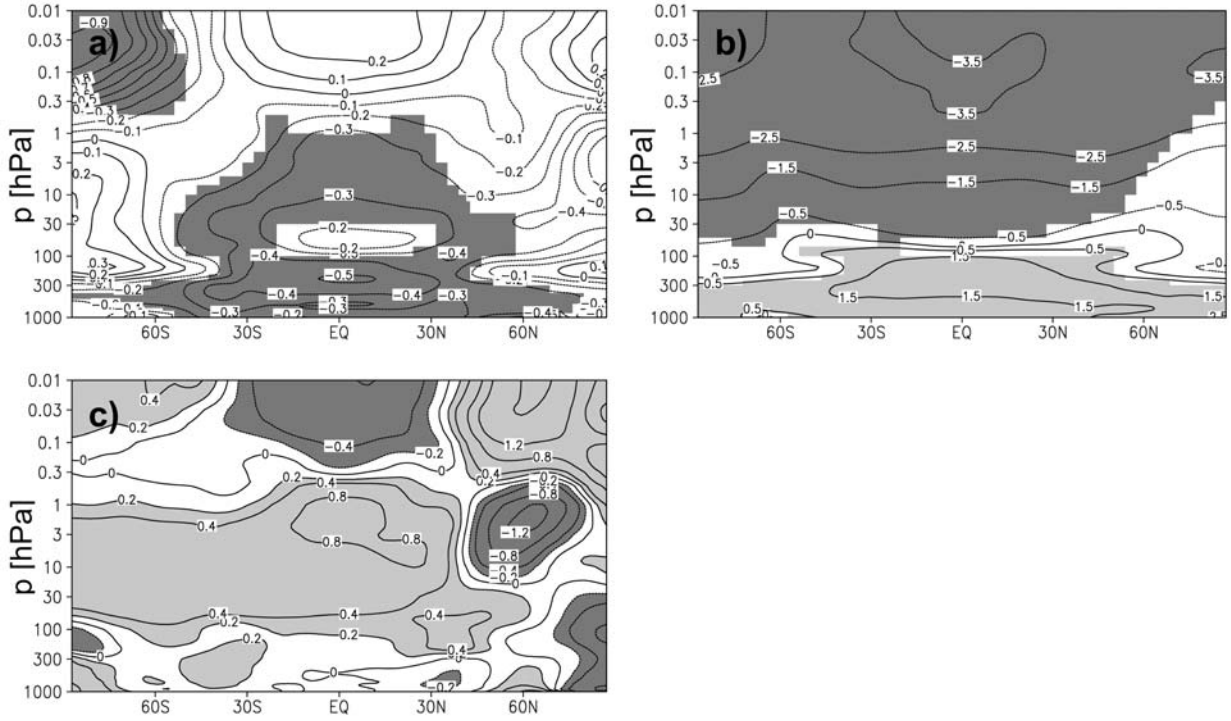

Figure 9. Climate change signal of zonal mean temperature (K). (a) LMM minus PI and (b) PD (1960–1990) minus LMM long-term annual mean difference in simulation including stratospheric solar ozone forcing (EGMAM-2). Grey shaded areas are statistically significant above 95th percentile value after Student's *t* test. (c) EGMAM-2 minus EGMAM-1 difference of the simulated climate change signals for PD (1960–1990) minus LMM (1675–1715) representing the solar signal in zonal mean temperature for boreal winter (DJF) due to changes in stratospheric ozone.

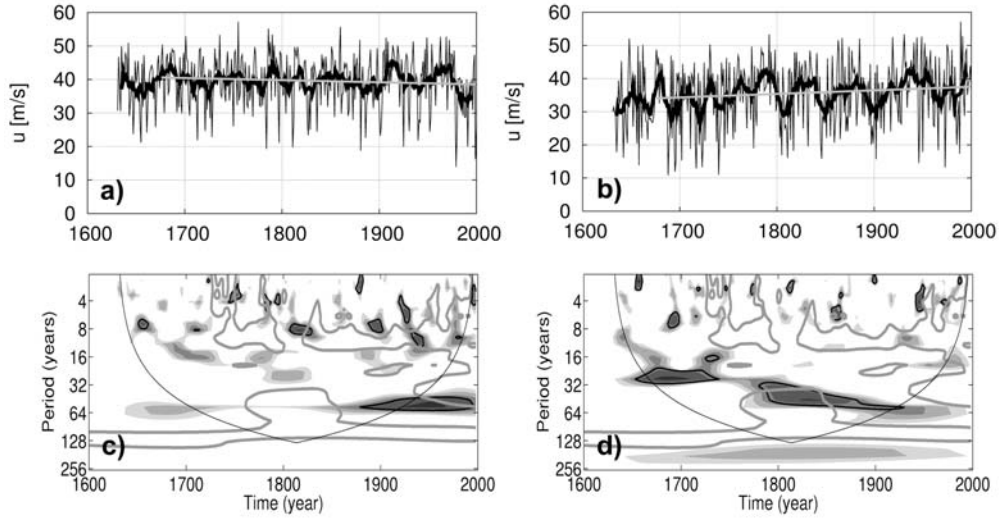

Figure 10. Winter (DJF) mean of zonal mean zonal wind (m/s) at 10 hPa, 60°N. (a) Simulation using fixed climatological ozone (EGMAM-1). (b) Simulation including solar stratospheric ozone forcing (EGMAM-2). Thick curve shows 11 year running mean. Wavelet power spectrum [after *Torrence and Compo*, 1998] of winter (DJF) mean of zonal mean zonal wind at 10 hPa, 60°N for (c) EGMAM-1 and (d) EGMAM-2. The Morlet wavelet is used. The oval curve indicates area of confidence as the variance is underestimated outside of this border. Thick black lines show 95% level of statistical significance (based on chi square test following *Torrence and Compo* [1998]) compared to stationary noise (redness estimate based on autocorrelation of the particular series). Thick grey lines show 95% area of statistical significance for corresponding wavelet analysis of solar forcing used to drive EGMAM and ECHO-G.

vortex is not evident in EGMAM-1 (Figure 10c). Moreover, the stratospheric ozone forcing is associated with a slight increase in vortex strength (Figure 10b). Here a positive linear trend of 1m/s per century is found for the time period from 1689 (the absolute minimum in solar activity; see Figure 1) until the end of the 20th century. The trend is statistically significant above the 90th percentile value according to a significance test after Mann-Kendall. A stronger stratospheric polar vortex during solar maximum is also obtained from 11 year cycle studies for QBO-east phase [e.g., *Labitzke et al.*, 2006; *Matthes et al.*, 2006]. Therefore, the long-term positive trend is in good agreement with the positive secular trend in solar activity (note that EGMAM simulates prevailing easterlies in the lower tropical stratosphere). These results indicate that the inclusion of solar induced changes in stratospheric ozone leads to more reasonable simulation of stratospheric variability. Together with results presented in the section 3.1, these findings support the hypothesis that a better representation of stratospheric variability also leads to more reasonable simulation of tropospheric variability on time scales from decades to centuries.

5. Discussion

[32] Simulations covering the time period from 1630 to 2000 AD are performed with a coupled AO-GCM including the middle atmosphere and compared to transient simulations performed with (1) the tropospheric version of this model and (2) a model that is based on completely different model formulations. This approach enables a separation of the role of the middle atmosphere for both the hemispheric and regional evolution of climate during the last centuries.

[33] A better representation of the middle atmosphere plays only a moderate role for simulating hemispheric scale variability, indicating that other aspects of model formulation are more important. With respect to regional changes, all simulations reveal a consistent cooling over large parts of the ocean in low latitudes during LMM compared with a pre-industrial time period. Since concentrations of well mixed GHGs are nearly constant for the period 1675–1790, this cooling can clearly be attributed to natural forcing (low solar activity, volcanic activity). Note that this cooling is in agreement with reconstructions [e.g., *Jones and Mann*, 2004; *Luterbacher et al.*, 2004]. However, the simulations are less consistent for mid and high latitudes. Employing a model including a detailed stratosphere, but neglecting the role of the deep ocean, *Shindell et al.* [2001, 2003] suggest that a shift of the NAO to a more negative phase during MM is related to lower solar activity. They also highlight the good agreement of the corresponding simulated and reconstructed (proxy based) near-surface temperature change pattern. In the coupled AO-GCM simulations presented in this study we also find a stronger cooling over Europe/Asia and less cooling or even warming over the western North Atlantic during LMM with respect to PI period. This is partly attributed to solar induced changes in atmospheric and oceanic circulation as proposed by earlier coupled AO-GCM studies [e.g., *Cubasch et al.*, 1997; *Zorita et al.*, 2004]. The model that uses better representation of volcanic forcing (CCSM3) also reveals a more negative NAO response for LMM with respect to the ensemble mean change indicating a response to the solar forcing. However, a clear, consistent shift of the NAO to a more negative phase during solar minima is not found for the individual simulations with EGMAM/ECHO-G/CCSM3 indicating that also internal variability plays a role for the simulated climate anomalies [cf. *Bengtsson et al.*, 2006]. Despite the lack of coherence between the different simulations there are distinct indications for a possible solar influence on the NAO. The simulation that includes a realistic representation of the stratosphere and solar induced stratospheric ozone forcing shows somewhat lower NAO values during the MM and the DM. However, these changes are not statistically significant for MM. An even stronger coherence between NAO and solar activity emerges for one simulation performed with the tropospheric version of the same model. This finding is similar to results by *Zorita et al.* [2004], who investigated a transient historical simulation performed with the same model suggesting a possible direct solar influence on the NAO (in contrast to an indirect effect involving the stratosphere). Though the vertically extended coupled GCM simulations reveal some indications for a possible indirect solar influence on NAO via the stratosphere, we conclude that a better representation of the stratosphere is not necessary to realistically reproduce the NAO response to solar forcing if comparably strong solar induced TSI changes are prescribed.

[34] Stronger evidence for a stratospheric effect on the tropospheric climate comes from assessment of climate change from LMM to PD, where strong increase in GHG concentrations and solar activity result in a comparatively strong forcing. Comparison of MSLP change patterns for the North Atlantic/European sector from LMM to PD reveals a NAO-like change toward stronger zonal flow over Western Europe in model simulations and reconstructions. Inclusion of both troposphere-stratosphere coupling processes and a more realistic stratospheric solar forcing contributes to a better agreement of the coupled AO-GCM simulations with reconstructed change in MSLP after *Luterbacher et al.* [2002]. We also find a clear effect of changes in stratospheric circulation on the simulated MSLP change patterns from LMM to PD over the eastern North Atlantic. However, the reconstructed MSLP over the North Atlantic is very uncertain due to sparse data. Improvement of the quality of the reconstructed MSLP over the North Atlantic (as for example by means of ship logs (J. Luterbacher, personal communication, 2008)) would therefore substantially contribute to better assessment of the simulated processes.

[35] The comparatively strong strengthening of the westerly flow over Western Europe in the simulations with the tropospheric version of the model is reduced to a more moderate level by including the dynamic troposphere-stratosphere coupling processes. Here, an increase in GHG concentrations is connected to a more disturbed stratospheric polar vortex at the end of the 20th century. A similar relationship between the level of GHG concentration and the strength of the polar stratospheric vortex is found in future climate projections using the same model [*Huebener et al.*, 2007; Schimanke et al., manuscript in preparation, 2010]. These studies report an increase in the number of sudden stratospheric warmings and a more disturbed stratospheric polar vortex under increasing GHG concentrations. Additionally, the more disturbed stratospheric polar vortex is related to a weakening of the tropospheric zonal flow via

downward propagating AO-negative like anomalies from the stratosphere to the troposphere [*Baldwin and Dunkerton*, 2001], partly compensating the comparatively strong increase in tropospheric westerlies as simulated in the tropospheric version of the model.

[36] By contrast, the inclusion of the stratospheric ozone forcing leads to a slight strengthening of the stratospheric polar vortex from MM to PD. Here, the secular trend in solar activity from MM to PD is connected to heating in the subtropical/tropical stratosphere and the entire summer hemisphere. This temperature change signal is similar to results from 11 year solar cycle studies for the solar maximum case [*Kodera and Kuroda*, 2002]. On the centennial time scale the stratospheric solar warming signal partly compensates the GHG induced stratospheric cooling.

[37] With respect to the response of stratospheric polar vortex strength to changes in solar activity a number of studies highlight the role of the background conditions even for the sign/direction of the change, for example, the state of the QBO and/or the level of atmospheric GHG concentrations. In our study the level of atmospheric GHG concentration may play a role [*Kodera et al.*, 2008], besides the state of the QBO [*Labitzke et al.*, 2006]. The effect may also be expressed conversely; that is, changes in vortex strength due to changes in well mixed GHG concentration may depend on solar activity as was shown by *Kodera et al.* [2008] in reanalysis data. In GCM simulations the setting of the gravity wave parameterization may also affect results [*Sigmond et al.*, 2008]. While *Charlton-Perez et al.* [2008] find an increase in the number of sudden stratospheric warmings on the basis of transient GHG scenario experiments, *Rind et al.* [1998] report a decrease in the number of sudden stratospheric warmings after doubling of CO_2 concentrations on the basis of idealized experiments.

[38] In the current study we present evidence that a better representation of the stratosphere in AO-GCMs not only significantly alters but also improves the simulation of regional climate when using coupled AO-GCMs. However, our study contains some shortcomings with respect to the external forcings used: (1) the simulations do not account for anthropogenic changes in sulphate aerosols [*Zorita et al.*, 2004]. (2) We did not explicitly account for changes in the UV part of the solar spectrum which is assumed to lead to more realistic representation of the solar signal due to direct short-wave radiative heating in the middle atmosphere and the resulting dynamic changes [*Langematz et al.*, 2005]. (3) The TSI changes that we used are within the range of uncertainty but strong when compared to some newer estimates of TSI [e.g., *Krivova et al.*, 2007].

[39] Because internal variability substantially contributes to the state of the polar stratospheric vortex with implications for tropospheric circulation also on longer time scales (Schimanke et al., manuscript in preparation, 2010) ensemble simulations are necessary. Moreover the uncertainty range to different solar forcings should be assessed by use of different reconstructions for total and spectral solar irradiance. For realistic representation of the solar response coupled AO-GCMs are needed which include realistic representation of the middle atmosphere and relevant processes. Examples of future improvement of current AO-GCMs are the representation of QBO variability and the interactive parameterized ozone chemistry. The recommended improvements will enable a better assessment of the role of solar forcing when compared to other natural and anthropogenic effects (e.g., GHG, volcanoes).

[40] **Acknowledgments.** The authors wish to thank Eduardo Zorita and J. Fidel González-Rouco for providing data from simulations with ECHO-G. Parts of this work were funded by the DFG project ProSEC-CO/CAWSES. We would like to thank Ulrike Langematz for helpful comments. The simulations with EGMAM and ECHO-G were performed on a NEC-SX6 supercomputer at "Deutsches Klimarechenzentrum" (DKRZ), Hamburg. Simulations with CCSM3 were performed at Swiss National Supercomputing Centre (CSCS). We would also like to thank the anonymous reviewers for their helpful comments.

References

Ammann, C. M., G. Meehl, W. Washington, and C. Zender (2003), A monthly and latitudinally varying volcanic forcing dataset in simulations of 20th century climate, *Geophys. Res. Lett.*, *30*(12), 1657, doi:10.1029/2003GL016875.

Ammann, C. M., F. Joos, D. S. Schimel, B. L. Otto-Bliesner, and R. A. Tomas (2006), Solar influence on climate during the last millennium: Results from transient simulations with the NCAR Climate System Model, *Proc. Natl. Acad. Sci. U. S. A.*, *104*, 3713–3718.

Baldwin, M. P., and T. J. Dunkerton (2001), Stratospheric harbingers of anomalous weather regimes, *Science*, *294*, 581–584.

Bengtsson, L., K. Hodges, E. Roeckner, and R. Brokopf (2006), On the natural variability of the pre-industrial European climate, *Clim. Dyn.*, *27*, 743–760, doi:10.1007/s00382-006-0168-y.

Blunier, T., J. A. Chappellaz, B. Stauffer, and D. Raynaud (1995), Variations in atmospheric methane concentration during the Holocene epoch, *Nature*, *374*, 46–49.

Briegleb, B., C. Bitz, W. Lipscomb, M. Holland, J. Schramm, and R. Moritz (2004), Scientific description of the sea ice component in the Community Climate System Model, version 3, *NCAR/TN-463+STR*, 70 pp., Natl. Cent. for Atmos. Res., Boulder, Colo.

Brühl, C. (1993), Atmospheric effects of stratospheric aircraft: Report of the 1992 Models and Measurements Workshop, *NASA Ref. Publ. 1292II*, 240 pp., NASA Goddard Space Flight Cent., Greenbelt, Md.

Bürger, G., I. Fast, and U. Cubasch (2006), Climate reconstruction by regression—32 variations on a theme, *Tellus, Ser. A*, *58*, 227–235.

Butchart, N., J. Austin, J. R. Knight, A. A. Scaife, and M. L. Gallani (2000), The response of the stratospheric climate to projected changes in the concentrations of well-mixed greenhouse gases from 1992 to 2051, *J. Clim.*, *13*, 2142–2159.

Casty, C., C. C. Raible, T. F. Stocker, H. Wanner, and J. Luterbacher (2007), A European pattern climatology 1766–2000, *Clim. Dyn.*, *29*, 791–805, doi:10.1007/s00382-007-0257-6.

Charlton-Perez, A. J., L. Polvani, J. Austin, and F. Li (2008), The frequency and dynamics of stratospheric sudden warmings in the 21st century, *J. Geophys. Res.*, *113*, D16116, doi:10.1029/2007JD009571.

Christiansen, T. B., T. Schmith, and P. Thejll (2009), A surrogate ensemble study of climate reconstruction methods: Stochasticity and robustness, *J. Clim.*, *21*, 951–976.

Collins, W. D., et al. (2006), The Community Climate Model version 3: CCSM3, *J. Clim.*, *19*, 2122–2143.

Crowley, T. J. (2000), Causes of climate change over the past 1000 years, *Science*, *289*, 270–277.

Cubasch, U., R. Voss, G. Hegerl, J. Waszkewitz, and T. Crowley (1997), Simulations of the influence of solar radiation variations on the global climate with an ocean-atmosphere general circulation model, *Clim. Dyn.*, *13*, 757–767.

Cubasch, U., G. A. Meehl, G. J. Boer, R. J. Stouffer, M. Dix, A. Noda, C. A. Senior, S. Raper, and K. S. Yap (2001), Projections of future climate change, in *Climate Change 2001: The Scientific Basis: Contribution of Working Group I to the Third Assessment Report of the Intergovernmental Panel on Climate Change*, edited by J. T. Houghton et al., pp. 526–582, Cambridge Univ. Press, Cambridge, U. K.

Cubasch, U., G. Bürger, I. Fast, T. Spangehl, and S. Wagner (2005), The direct solar influence of cliamte: modeling the lower atmosphere, *Mem. Soc. Astron.*, *76*, 810–818.

Dlugokencky, E., S. Houweling, L. Bruhwiler, K. Masarie, P. Lang, J. Miller, and P. Tans (2003), Atmospheric methane levels off: Temporary pause or a new steady-state?, *Geophys. Res. Lett.*, *30*(19), 1992, doi:10.1029/2003GL018126.

Etheridge, D., L. P. Steele, L. Langefelds, R. J. Francey, J. M. Barnola, and V. I. Morgan (1996), Natural and anthropogenic changes in atmospheric

CO_2 over the last 1000 years from air in Antarctic ice and firn, *J. Geophys. Res.*, *101*, 4115–4128.

Fischer-Bruns, I., U. Cubasch, H. von Storch, E. Zorita, J. F. González-Rouco, and J. Luterbacher (2002), Modelling the Late Maunder Minimum with a 3-dimensional Ocean-Atmosphere GCM, *CLIVAR Exchanges*, *7*, 59–61.

Flückiger, J. A., A. Dallenbach, T. Blunier, B. Stauffer, T. Stocker, D. Raynaud, and J. Barnola (1999), Variations in atmospheric N_2O concentration during abrupt climatic change, *Science*, *285*, 227–230.

Flückiger, J. A., E. Monnin, B. Stauffer, J. Schwander, T. Stocker, J. Chappellaz, D. Raynaud, and J. Barnola (2002), High-resolution Holocene N2O ice core record and its relationship with CH4 and CO2, *Global Biogeochem. Cycles*, *16*(1), 1010, doi:10.1029/2001GB001417.

González-Rouco, J. F., H. Beltrami, E. Zorita, and H. von Storch (2006), Simulation and inversion of borehole temperature profiles in surrogate climates: Spatial distribution and surface coupling, *Geophys. Res. Lett.*, *33*, L01703, doi:10.1029/2005GL024693.

Hoyt, D. V., and K. H. Schatten (1993), A discussion of plausible solar irradiance variations, 1700–1992, *J. Geophys. Res.*, *98*, 18,895–18,906.

Huebener, H., U. Cubasch, U. Langematz, T. Spangehl, F. Niehörster, I. Fast, and M. Kunze (2007), Ensemble climate simulations using a fully coupled ocean-troposphere-stratosphere general circulation model, *Philos. Trans. R. Soc., Ser. A*, *365*, 2089–2101.

Intergovernmental Panel on Climate Change (IPCC) (2007), *Climate Change, The Physical Science Basis, Contribution of Working Group I to the Fourth Assessment Report of the Intergovernmental Panel on Climate Change*, edited by S. Solomon et al., Cambridge Univ. Press., Cambridge, U. K.

Jones, P. D., and M. E. Mann (2004), Climate over past millennia, *Rev. Geophys.*, *42*, RG2002, doi:10.1029/2003RG000143.

Jones, P. D., T. Jonsson, and D. Wheeler (1997), Extension to the North Atlantic Oscillation using early instrumental pressure observations from Gibraltar and south-west Iceland, *Int. J. Climatol.*, *17*, 1433–1450.

Kaspar, F., T. Spangehl, and U. Cubasch (2007), Northern Hemisphere winter storm tracks of the Eemian interglacial and the last glacial inception, *Clim. Past*, *3*, 181–192.

Keeling, C. D., and T. P. Whorf (2005), Atmospheric CO_2 records from sites in the SIO air sampling network, in *Trends: A Compendium of Data on Global Change*, pp. 16–26, Carbon Dioxide Inf. Anal. Cent., Oak Ridge Natl. Lab., U.S. Dep. of Energy, Oak Ridge, Tenn.

Kelly, P. M., and T. M. L. Wigley (1992), Solar cycle length greenhouse forcing and global climate, *Nature*, *360*, 328–330.

Kiehl, J. T., C. A. Shields, J. J. Hack, and W. D. Collins (2006), The climate sensitivity of the Community Climate System Model version 3 (CCSM3), *J. Clim.*, *19*, 2584–2596.

Kodera, K., and Y. Kuroda (2002), Dynamical response to the solar cycle, *J. Geophys. Res.*, *107*(D24), 4749, doi:10.1029/2002JD002224.

Kodera, K., M. E. Hori, S. Yukimoto, and M. Sigmond (2008), Solar modulation of the Northern Hemisphere winter trends and its implications with increasing CO_2, *Geophys. Res. Lett.*, *35*, L03704, doi:10.1029/2007GL031958.

Körper, J., T. Spangehl, H. Huebener, and U. Cubasch (2009), Decomposition of Projected regional sea level rise in the North Atlantic and its relation to the AMOC, *Geophys. Res. Lett.*, *36*, L19714, doi:10.1029/2009GL039757.

Krivova, N. A., L. Balmaceda, and S. K. Solanki (2007), Reconstruction of solar total irradiance since 1700 from the surface magnetic flux, *Astron. Astrophys.*, *467*, 335–346, doi:10.1051/0004-6361:20066725.

Kuroda, Y., and K. Kodera (2002), Effect of solar activity on the polar-night jet oscillation in the Northern and Southern Hemisphere winter, *J. Meteorol. Soc. Jpn.*, *80*(4B), 973–984.

Labitzke, K., M. Kunze, and S. Brönnimann (2006), Sunspots, the QBO, and the stratosphere in the North Polar Region—20 years later, *Meteorol. Z.*, *15*, 355–363.

Langematz, U., A. Clausnitzer, K. Matthes, and M. Kunze (2005), The climate during the Maunder Minimum: A simulation with the Freie Universität Berlin Climate Middle Atmosphere Model (FUB-CMAM), *J. Atmos. Sol. Terr. Phys.*, *67*, 55–69.

Langematz, U., P. Sinigoj, T. Spangehl, B. Ayarzagüena, and U. Cubasch (2009), Stratosphere-troposphere dynamical coupling: A robust coupled mode of the Earth's atmosphere?, paper presented at Our Warming Planet: MOCA-09, Int. Assoc. of Meteorol. and Atmos. Sci., Montreal, Que., Canada.

Lean, J., J. Beer, and R. Bradley (1995), Reconstruction of solar irridiance since 1610: Implications for climate change, *Geophys. Res. Lett.*, *22*, 3195–3198.

Legutke, S., and R. Voss (1999), The Hamburg Atmosphere-Ocean Coupled Circulation Model ECHO-G, *Tech. Rep. 18*, Dtsch. Klimarechenzentrum, Hamburg, Germany.

Luterbacher, J., R. Rickli, E. Xoplaki, C. Tunkuely, C. Beck, C. Pfister, and H. Wanner (2001), The Late Maunder Minimum (1675–1715)—A key period for studying decadal scale climatic change in Europe, *Clim. Change*, *49*, 441–462.

Luterbacher, J., E. Xoplaki, D. Dietrich, R. Rickli, J. Jacobeit, C. Beck, D. Gylistras, C. Schmutz, and H. Wanner (2002), Reconstruction of sea-level pressure fields over the eastern North Atlantic and Europe back to 1500, *Clim. Dyn.*, *18*, 545–561.

Luterbacher, J., D. Dietrich, E. Xoplaki, M. Grosjean, and H. Wanner (2004), European seasonal and annual temperature variability, trends and extremes since 1500, *Science*, *303*, 1499–1503.

Mann, M. E., S. Rutherford, E. Wahl, and C. Ammann (2007a), Reply to comments on "Testing the fidelity of methods used in proxy-based reconstructions of past climate," *J. Clim.*, *20*, 3699–3703.

Mann, M. E., S. Rutherford, E. Wahl, and C. Ammann (2007b), Robustness of proxy-based climate field reconstruction methods, *J. Geophys. Res.*, *112*, D12109, doi:10.1029/2006JD008272.

Manzini, E., and N. A. M. Farlane (1998), The effect of varying the source spectrum of a gravity wave parameterization in a middle atmosphere general circulation model, *J. Geophys. Res.*, *103*, 31,523–31,539, doi:10.1029/98JD02274.

Matthes, K., Y. Kuroda, K. Kodera, and U. Langematz (2006), Transfer of the solar signal from the stratosphere to the troposphere: Nothern winter, *J. Geophys. Res.*, *111*, D06108, doi:10.1029/2005JD006283.

Meehl, G. A., J. M. Arblaster, K. Matthes, F. Sassi, and H. van Loon (2009), Amplifying the Pacific climate system response to a small 11-year solar cycle forcing, *Science*, *325*, 1114–1118.

Min, S.-K., S. Legutke, A. Hense, and W.-T. Kwon (2005a), Internal variability in a 1000-yr control simulation with the coupled climate model ECHO-G—I. Near-surface temperature, precipitation and mean sea level pressure, *Tellus, Ser. A*, *57*, 605–621.

Min, S.-K., S. Legutke, A. Hense, and W.-T. Kwon (2005b), Internal variability in a 1000-yr control simulation with the coupled climate model ECHO-G—II. El Nino Southern Oscillation and North Atlantic Oscillation, *Tellus, Ser. A*, *57*, 622–640.

Oleson, K. W., et al. (2004), 2004Technical description of the Community Land Model (CLM), *NCAR/TN-461+STR*, 173 pp., Natl. Cent. for Atmos. Res., Boulder, Colo.

Osborn, T. (2004), Simulating the winter North Atlantic Oscillation: The roles of internal variability and greenhouse gas forcing, *Clim. Dyn.*, *22*, 605–623.

Osborn, T., S. C. B. Raper, and K. Briffa (2006), Simulated climate change during the last 1,000 years: Comparing the ECHO-G circulation model with the MAGICC simple climate model, *Clim. Dyn.*, *27*, 185–197, doi:10.1007/s00382-006-0129-5.

Raible, C. C., U. Luksch, K. Fraedrich, and R. Voss (2001), North Atlantic decadal regimes in a coupled GCM simulation, *Clim. Dyn.*, *18*, 321–330.

Raible, C. C., T. F. Stocker, M. Yoshimori, M. Renold, U. Beyerle, and C. Casty (2005), Northern Hemisphere trends of pressure indices and atmospheric circulation patterns in observations, reconstructions, and coupled GCM simulation, *J. Clim.*, *18*, 3968–3982.

Raible, C. C., M. Yoshimori, T. F. Stocker, and C. Casty (2007), Extreme midlatitude cyclones and their implications for precipitation and wind speed extremes in simulations of the Maunder Minimum versus present day conditions, *Clim. Dyn.*, *28*, 409–423.

Ramaswamy, V., O. Boucher, J. Haigh, D. Hauglustaine, J. Haywood, G. Myhre, T. Nakajima, G. Shi, and S. Solomon (2001), Radiative forcing of climate change, in *Climate Change 2001: The Scientific Basis: Contribution of Working Group I to the Third Assessment Report of the Intergovernmental Panel on Climate Change*, edited by J. T. Houghton et al., pp. 351–416, Cambridge Univ. Press, Cambridge, U. K.

Rind, D., D. Shindell, P. Lonergan, and N. K. Balachandran (1998), Climate Change and the middle atmosphere. Part III: The doubled CO_2 climate revisited, *J. Clim.*, *11*, 876–894.

Rind, D., D. Shindell, J. Perlwitz, J. Lerner, P. Lonergan, J. Lean, and C. McLinden (2004), The relative importance of solar and anthropogenic forcing of climate change between the Maunder Minimum and present, *J. Clim.*, *17*, 906–929.

Rind, D., J. Perlwitz, and P. Longeran (2005), AO/NAO response to climate change: 1. Respective influences of stratospheric and tropospheric climate changes, *J. Geophys. Res.*, *110*, D12107, doi:10.1029/2004JD005103.

Roeckner, E., K. Arpe, L. Bengtsson, M. Claussen, L. Dümenil, M. Esch, M. Giorgetta, U. Schlese, and U. Schulzweida (1996), The Atmospheric General Circulation Model ECHAM-4: Model description and simulation of present-day climate, *MPI Rep. 218*, Max-Planck-Inst. für Meteorol., Hamburg, Germany.

Shindell, D. T., G. A. Schmidt, M. E. Mann, D. Rind, and A. Waple (2001), Solar forcing of regional climate change during the Maunder Minimum, *Science*, *294*, 2149–2152.

Shindell, D. T., G. A. Schmidt, R. L. Miller, and M. E. Mann (2003), Volcanic and solar forcing of climate change during the preindustrial era, *J. Clim.*, *16*, 4094–4107.

Sigmond, M., P. Siegmund, E. Manzini, and H. Kelder (2004), A simulation of the separate climate effects of middle-atmospheric and tropospheric CO_2 doubling, *J. Clim.*, *17*, 2352–2367.

Sigmond, M., J. Scinocca, and P. J. Kushner (2008), Impact of the stratosphere on tropospheric climate change, *Geophys. Res. Lett.*, *35*, L12706, doi:10.1029/2008GL033573.

Smith, R., and P. Gent (2004), Reference manual for the Parallel Ocean Programme (POP), ocean component of the Community Climate System Model (CCSM2.0 and 3.0), *Tech. Rep. LA-UR-2484*, 75 pp., Los Alamos Natl. Lab., Los Alamos, N. M.

Stendel, M., I. A. Mogensen, and J. H. Christensen (2006), Influence of various forcings on global climate in historical times using a coupled atmosphere-ocean general circulation model, *Clim. Dyn.*, *26*, 1–15, doi:10.1007/s00382-005-0041-04.

Stephenson, D. B., P. Pavan, M. Collins, M. M. Junge, and R. Quadrelli (2006), North Atlantic Oscillation response to transient greenhouse gas forcing and the impact on European winter climate: A CMIP2 multi-model assessment, *Clim. Dyn.*, *27*, 401–420.

Taylor, K. E. (2001), Summarizing multiple aspects of model performance in a single diagram, *J. Geophys. Res.*, *106*, 7183–7192.

Tett, S. F. B., R. Betts, T. J. Crowley, J. Gregory, T. C. Johns, T. J. Osborn, E. Öström, D. L. Roberts, and M. J. Woodage (2007), The impact of natural and anthropogenic forcings on climate and hydrology since 1550, *Clim. Dyn.*, *28*, 3–34, doi:10.1007/s00382-006-0165-1.

Thompson, T. M., et al. (2004), Halocarbons and other atmospheric trace species, *Summary Rep. 27*, Clim. Monit. and Diagn. Lab., Boulder, Colo.

Torrence, C., and G. P. Compo (1998), A practical guide to wavelet analysis, *Bull. Am. Meteorol. Soc.*, *79*, 61–78.

Uppala, S., et al. (2005), The ERA-40 reanalysis, *Q. J. R. Meteorol. Soc.*, *131*, 2961–3012.

von Storch, H., E. Zorita, J. M. Jones, Y. Dimitriev, F. González-Rouco, and S. F. B. Tett (2004), Reconstructing past climate from noisy data, *Science*, *306*, 679–682.

Wagner, S., and E. Zorita (2005), The influence of volcanic, solar and CO_2 forcing on the temperatures in the Dalton Minimum (1790–1830), *Clim. Dyn.*, *25*, 205–218, doi:10.1007/s00382-005-0029-0.

Wang, Y., J. Lean, and N. Sheeley (2005), Modeling the Sun's magnetic field and irradiance since 1713, *Astrophys. J.*, *625*, 522–538.

William, W. D. C., P. J. Rasch, B. A. Boville, J. J. Hack, J. R. McCaa, D. L. Williamson, B. P. Briegleb, C. M. Bitz, S.-J. Lin, and M. Zhang (2006), The formulation and atmospheric simulation of the Community Atmosphere Model version 3: CAM3, *J. Clim.*, *19*, 2144–2161.

Wolff, J., E. Maier-Reimer, and S. Legutke (1997), The Hamburg Ocean Primitive Equation Model, *Tech. Rep. 13*, Dtsch. Klimarechenzentrum, Hamburg, Germany.

Yeager, S., C. A. Shields, W. G. Larege, and J. J. Hack (2006), The low-resolution CCSM3, *J. Clim.*, *19*, 2454–2566.

Yoshimori, M., T. F. Stocker, C. C. Raible, and M. Renold (2005), Externally forced and internal variability in ensemble climate simulations of the Maunder Minimum, *J. Clim.*, *18*, 4253–4270.

Yoshimori, M., C. C. Raible, T. F. Stocker, and M. Renold (2006), On the interpretation of low-latitude hydrological proxy records based on Maunder Minimum AOGCM simulations, *Clim. Dyn.*, *27*, 493–513.

Yoshimori, M., C. C. Raible, T. F. Stocker, and M. Renold (2010), Simulated decadal oscillations of the Atlantic meridional overturning circulation in a cold climate state, *Clim. Dyn.*, *31*, 101–121, doi:10.1007/s00382-009-0540-9.

Zorita, E., H. von Storch, F. González-Rouco, U. Cubasch, J. Luterbacher, S. Legutke, I. Fischer-Bruns, and U. Schlese (2004), Climate evolution in the last five centuries simulated by an atmosphere-ocean model: Global tempertures, the North Atlantic Oscillation and the Late Maunder Minimum, *Meteorol. Z*, *13*, 271–289.

Zorita, E., J. F. González-Rouco, H. von Storch, J. P. Montavez, and F. Valero (2005), Natural and anthropogenic modes of surface temperature variations in the last thousand years, *Geophys. Res. Lett.*, *32*, L08707, doi:10.1029/2004GL021563.

Zorita, E., F. González-Rouco, and H. von Storch (2007), Comments to "Testing the fidelity of methods used in proxy-based reconstructions of past climate" by Mann et al., *J. Clim.*, *20*, 3693–3698, doi:10.1175/JCLI4171.1.

U. Cubasch, J. Körper, S. Schimanke, and T. Spangehl, Institut für Meteorologie, Freie Universität Berlin, Carl-Heinrich-Becker-Weg 6-10, D-12167 Berlin, Germany. (spangehl@met.fu-berlin.de)

D. Hofer and C. C. Raible, Climate and Environmental Physics, Physics Institute, University of Bern, Sidlerstr. 5, CH-3012 Bern, Switzerland.